American Mineralogist, Volume 81, pages 1057–1079, 1996

Rigid-unit phonon modes and structural phase transitions in framework silicates

KENTON D. HAMMONDS,[1] MARTIN T. DOVE,[1,*] ANDREW P. GIDDY,[2]
VOLKER HEINE,[2] AND BJÖRN WINKLER[3]

[1]Department of Earth Sciences, University of Cambridge, Downing Street, Cambridge CB2 3EQ, U.K.
[2]Cavendish Laboratory, University of Cambridge, Madingley Road, Cambridge CB3 0HE, U.K.
[3]Mineralogisches Institut der Christian-Albrechts Universität, Olshausenstrasse 40, D-24098 Kiel, Germany

ABSTRACT

The rigid-unit mode model provides many new insights into the stability and physical properties of framework silicates. In this model the SiO_4 and AlO_4 tetrahedra are treated as very stiff, to a first approximation as completely rigid, in comparison with intertetrahedral forces. In this paper we apply the model to several important examples. The model is reviewed by a detailed study of quartz, and it is shown that the α-β phase transition involves a rigid-unit mode that preserves the Si-O-Si bond angle. The model is used to explain the phase transitions in cristobalite and the different feldspar, sodalite, and leucite structures. We also use the model to explain the nature of the high-temperature disordered phases of cristobalite and tridymite, to interpret the observations of streaks of diffuse scattering in electron diffraction patterns, to interpret the structures in the kalsilite-nepheline solid solution, to explain volume anomalies in the cubic leucite structures, and to explain qualitatively the negative linear thermal expansion in cordierite. The results for the highest symmetry sodalite structure show that there is a rigid-unit mode at every wave vector, a finding with significant implications for the understanding of the sorption and catalytic behavior of zeolites.

INTRODUCTION

Over the past decade a lot of work has been concerned with characterizing the structural, thermodynamic, and kinetic properties of phase transitions in minerals. One successful approach has been the use of Landau theory to provide a thermodynamic framework with which to link a wide range of observations (see, for example, Salje 1990). But little attention has been paid to the general question of why these phase transitions occur, and to specific issues such as why Landau theory often provides a good description of the behavior associated with a phase transition over a wide range of temperatures, including close to the transition temperature (Dove et al. 1992; Dove 1997).

Some of these issues can be tackled by starting with the simple observation that the forces that operate within SiO_4 and AlO_4 tetrahedra are much stronger than the forces that act between these tetrahedra, such as the force associated with the bending of the Si-O-Si bond. The starting point is a simple, yet instructive model in which the tetrahedra are assumed to be completely rigid. The next stage in this model is to include the forces that allow deformation of the tetrahedra and the weaker forces that operate between tetrahedra. From the simplest version of this model there follows, for example, an explanation of why displacive phase transitions are so common in framework silicates, the realization that the transition temperatures are simply related to the stiffness of the tetrahedra, and an understanding of why many displacive phase transitions can be described by Landau theory (Dove et al. 1991, 1992, 1995; Dove 1997). These, and several other results, have been obtained in the general case, and it is clear from the formulation that the results are applicable to any silicate, but they have been tested in detail only for the α-β phase transition in quartz (Vallade et al. 1992; Tautz et al. 1991; Dove et al. 1995, and in preparation). It is the purpose of this paper to apply these ideas to several important silicates.

The essential feature in our model is the concept of the rigid-unit mode (abbreviated as RUM). This is a vibrational mode that can propagate in a framework structure with no distortion of the tetrahedra, which rotate and translate as rigid units (Dove et al. 1991, 1992; Giddy et al. 1993). These modes have low frequencies and are therefore candidates for the classical soft modes associated with displacive phase transitions. In general, RUMs are thermally excited, but they can also lead to static distortions of any structure in different ways to accommodate large or small cations (Dove et al. 1991, 1996a). Thus, the RUM model can be applied directly to the two problems of displacive phase transitions and cation-ordering phase transitions. To some extent the RUM model is closely related to the "polyhedral-tilting" description

* Author to whom all correspondence should be addressed.

0003–004X/96/0910–1057$05.00

of phase transitions (Hazen and Finger 1982). We further aimed to develop a method for calculating all possible RUM distortions of a framework structure (Giddy et al. 1993; Hammonds et al. 1994), to recognize the implications of the existence of RUMs as vibrational modes of motion and of their role in generating the static distortions of the structure (Dove et al. 1991, 1995, 1996a), and to link the finite stiffness of the tetrahedra to a broad range of phenomena in a single model (Dove et al. 1993, 1995).

In the present paper we consider several examples of structures to highlight features of the RUM model. A discussion of the background of the RUM model, including its relationship to earlier models and the methods we developed to calculate the RUM spectrum for any given structure, is provided in the next section. The following sections discuss several examples that illustrate and develop different features of the model. These show how the RUM model can be used to explain (1) the occurrence of displacive phase transitions, (2) the effect of a phase transition on measured phonon frequencies, (3) the nature of high-temperature phases, (4) the observations of strong streaks of diffuse scattering in electron diffraction, (5) the way a structure relaxes to accommodate cation ordering, (6) how we can distinguish between elastic instabilities and displacive phase transitions involving soft optic phonons, (7) the dependence of a displacive phase transition on chemical composition, (8) the reasons why Landau theory should be directly applicable to the displacive phase transitions found in aluminosilicates, (9) the possibility of having local distortions of open structures typified by zeolites without significant distortions of neighboring regions, (10) how the size of cations in structural cages affects the volume of a structure, and (11) the possibility of negative thermal expansion. Because of the wide scope of phenomena we describe, no attempt is made to cover every aspect of each structure in depth. Rather, we use the different structures to introduce and discuss certain ideas that have wider applicability because they are more clearly seen in these structures or for some other reason such as the availability of experimental data or detailed calculations. Because our computer program for calculating the RUM spectra of framework structures is freely available, some of the other details are left for the interested reader to pursue in more depth. Indeed, one of our aims in the present work is to stimulate others to apply RUM analysis to other structures.

In this paper we mostly restrict our attention to RUMs with special wave vectors, whether special points, along symmetry axes, or on planes of symmetry. Intuitively we might expect that RUMs would be found only for special wave vectors, and this intuition is partly supported by our analysis, but we found examples of the occurrence of RUMs on curved lines or surfaces of wave vectors that have no relationship to the symmetry axes. Because one of the main objectives in this paper is to relate the RUM spectra to displacive phase transitions—and generally displacive phase transitions involve an instability at a special wave vector—we mostly report the RUM spectra for special wave vectors.

Rigid tetrahedra and the concept of the rigid-unit mode (RUM)

Summary of previous related work

Since the first X-ray diffraction studies of silicates, it has been recognized that the strength of the SiO_4 tetrahedra plays an important role in both the structure and stability of any framework silicate. For a long time this fact has been exploited in the distance least-squares tool for the prediction of new silicate crystal structures. Recent ab initio calculations of the bonding of silicates have shown that the force constants associated with stretching of the Si-O bonds and bending of the O-Si-O bond angles are much stronger than the interactions between neighboring tetrahedra (e.g., Lasaga and Gibbs 1987, 1988), such as the force constant for bending of the Si-O-Si bond angle. Computational methods such as lattice-energy minimization techniques frequently use transferable potentials for silicates (Dove 1989; Winkler et al. 1991; Patel et al. 1991), which reflects the common experience that the Si-O bond length is nearly a universal quantity. Crystal fields always give a small perturbation of the shape of the tetrahedra, but these effects are usually on the order of only 1% at most, and recent analysis of the displacement parameters measured in crystal-structure analysis has confirmed that the largest components of thermal motion involve the tetrahedra moving as rigid units (Downs et al. 1990, 1992; Boisen et al. 1990; Gibbs et al. 1994).

It has long been recognized that the tetrahedra usually retain their size and shape when a framework silicate undergoes a displacive phase transition. Megaw (1973) discussed this point at some length. She included in her examples the α-β phase transition in quartz and the distortions of the $C2/m$ feldspar structure from an idealized structure by rotations of the tetrahedra that do not break the symmetry. These ideas were further quantified by Grimm and Dorner (1975) in their analysis of the phase transition in quartz. By assuming that the tetrahedra were perfectly rigid these authors were able to define all the changes in the structure on the basis of one parameter (a rotation angle), which could be identified with the order parameter, and they found that the observed structural changes follow the predictions of the rigid tetrahedra model remarkably well. The only difficulty with this approach was that the model gave values for the unit-cell parameters that were too large at high temperatures, a point that we will comment on later.

Grimm and Dorner (1975) were the first to note that the soft mode for the phase transition in quartz should also involve the tetrahedra moving as rigid units, given that the atomic motions associated with the soft mode should correspond to the displacements associated with the phase transition. This point has been developed in later lattice-dynamics studies of quartz (Boysen et al. 1980;

Berge et al. 1986; Bethke et al. 1987; Dolino et al. 1989, 1992; Vallade et al. 1992). From inelastic neutron-scattering measurements of the α phase of quartz, Boysen et al. (1980) observed a mode at wave vector (½,0,0) of M_2 symmetry that softens considerably on heating to the phase transition. These measurements were found to be consistent with a model in which the atomic motions associated with the M_2 phonon in the high-temperature phase of quartz perfectly preserve the shape and size of the SiO_4 tetrahedra. However, we show below that in the low-temperature phase this mode must involve distortions of the tetrahedra, which accounts for the high frequency at low temperatures.

Vallade and coworkers (Berge et al. 1986; Vallade et al. 1992) were the first to realize that the idea of lattice vibrations in which the SiO_4 tetrahedra move as rigid units may have some important quantitative implications beyond the simple empirical observation. These workers were interested in the transition to the incommensurate phase that exists over a temperature range of 1.5 K between the α and β phases and found that the incommensurate instability could arise as a natural consequence of the existence of a line of RUMs on the branch between (0,0,0) and (½,0,0). To demonstrate this point, Vallade calculated the complete set of RUMs for all special and general wave vectors (Berge et al. 1986; Vallade et al. 1992).

The RUM idea has been explored in some detail in the study of glasses (Döhler et al. 1980; Thorpe 1983; He and Thorpe 1985; Cai and Thorpe 1989), in which the RUMs are called "floppy modes" (Buchenau et al. 1984, 1986). The analysis of floppy modes in glasses has been based on topology and the balance between the number of degrees of freedom, F, and the number of constraints, C (Marians and Burdett 1990; Marians and Hobbs 1990a, 1990b). The number of floppy modes in any system is equal to $F - C$. The existence of floppy modes has been shown to account for the existence of glass formation as a function of chemical composition and for the low-temperature transport properties of glasses. For networks of connected tetrahedra there are six degrees of freedom per tetrahedron (three translations and three rotations), and in the simplest way of counting constraints there are three constraint equations associated with the positions of each vertex linking two connected tetrahedra. Because these three constraints are shared by two tetrahedra, and there are four vertices in a tetrahedron, there are six constraints per tetrahedron. Hence, the simple application of these ideas to framework silicate crystals leads to the prediction that $F = C$, which suggests that silicates are finely balanced, neither underconstrained nor overconstrained, with the number of rigid-unit modes being exactly zero. However, we demonstrated elsewhere (Dove et al. 1992, 1996a; Giddy et al. 1993) that symmetry can cause some constraints to be degenerate and hence no longer independent. This means that $F - C$ is no longer zero, and a finite number of rigid-unit modes is present, although the number may be small in comparison with the total number of normal modes in the crystal. In any case, silicates represent the marginal case, having neither completely rigid frameworks with $C > F$ nor being completely floppy with $C \ll F$. Instead, it is generally the case that $C \leq F$ with only a few rigid-unit modes, indeed on the order of zero in comparison with the total number of modes, but we report some examples in this paper where the number of rigid-unit modes is, perhaps surprisingly, relatively large.

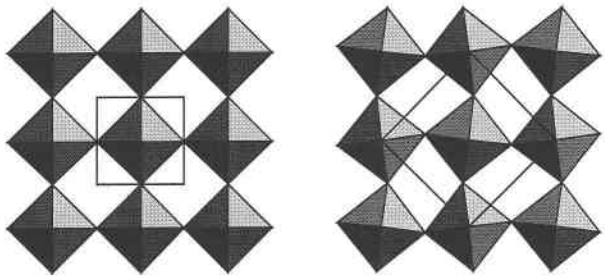

FIGURE 1. Polyhedral representation of an idealized two-dimensional perovskite structure, showing the open high-symmetry structure (**left**) and the collapsed lower symmetry structure formed by rotations of the polyhedra (**right**). The outlines of the unit cells are marked in both cases, highlighting the change in the unit cell that results from the phase transition.

Optic and acoustic modes

The RUM in quartz that acts as the soft mode for the α-β phase transition is an optic mode, as are many of the RUMs discussed in this paper. However, it is also possible to have acoustic RUMs other than the expected three acoustic modes with $\omega = 0$ at $k = 0$, i.e., the three uniform translations. In one type of acoustic RUM the acoustic mode is a RUM for all wave vectors between $k = 0$ and a zone-boundary point. In a second type of acoustic RUM the acoustic mode frequency varies as $\omega \propto k^2$ rather than as $\omega \propto k$. This implies that an elastic constant (or appropriate combination of elastic constants) is zero. The RUM is then better described as a strain distortion rather than as a phonon distortion. Either of these two types of acoustic RUMs can act as soft modes for ferroelastic phase transitions. However, the distinction between acoustic and optic modes is technically possible only in the limit $\mathbf{k} \rightarrow 0$ because away from this limit it is commonly found that some optic distortions can mix into the acoustic modes.

Example of perovskite

It is useful to illustrate some of the essential ideas outlined above with reference to the perovskite structure idealized as a framework of connected octahedra. Figure 1 shows part of a two-dimensional layer. If motion is restricted to only two dimensions, there are ways that the octahedra can move without distorting. The first two are the uniform translations along two orthogonal directions, which correspond to the $\mathbf{k} = 0$ acoustic modes. The third is the uniform rotation of the whole sample. The fourth type of motion, which is the important motion in the

present context, is the rotation of the octahedra in which neighbors rotate in equal and opposite senses as illustrated in Figure 1. This is a RUM that corresponds to a rotational phonon with wave vector (½,½) in the two-dimensional Brillouin zone. In three dimensions, the layers above and below can distort in the same way, but because there is no coupling between layers for this motion the relative phase between layers is arbitrary. Thus, there is a RUM involving rotation about [001] for every wave vector along the line (½,½,ξ) in reciprocal space, and also along the symmetry-related directions along the edges of the cubic Brillouin zone. Where these lines intersect at the corners there is a triply degenerate RUM. This picture has been discussed in more depth by Giddy et al. (1993) and Sollich et al. (1994).

In the low-temperature phase, illustrated in Figure 1, the octahedra can rotate only if there is a corresponding linear change in the unit-cell size. The fact that the RUMs are normal modes of vibration implies that any changes in volume couple with the RUM displacements only to higher order. Thus, in the low-temperature distorted phase the rotational mode is no longer a RUM. In general there are fewer RUMs in lower symmetry phases, which follows from the fact that lower symmetry leads to fewer degenerate constraints and hence a reduction in the number of allowed RUMs. In three dimensions, if the structure distorts at the phase transition by rotations of the octahedra about [0,0,1], the only RUMs that remain are for wave vectors (ξ,0,0) and (0,ξ,0).

This simple RUM description of the rotational phonons in the perovskite structure is supported experimentally for systems like $SrTiO_3$. Inelastic neutron-scattering measurements (Stirling 1972) have shown that the phonons all along the RUM lines have low frequencies, whereas the phonons for wave vectors away from these lines have rapidly increasing frequencies. The phase transition in $SrTiO_3$ involves a softening of the triply degenerate RUM at (½,½,½). The whole line of RUMs softens uniformly on cooling toward the transition temperature, but the RUM frequency at (½,½,½) is slightly lower than at (½,½,0), so the instability occurs first at (½,½,½).

The example of the perovskite structure illustrates several important ideas that recur throughout our different examples of framework aluminosilicates in this paper. First, the soft mode for the phase transition is a RUM. Second, RUMs are not restricted to single wave vectors but can occur along lines in reciprocal space. Indeed, in some examples RUMs occur for planes of wave vectors, and in one example there is one RUM for each wave vector throughout the Brillouin zone. Third, the change in symmetry that is caused by a phase transition also results in a change in the number of allowed RUMs. This is due to a corresponding decrease in the degeneracies of the constraints alluded to above.

The example of perovskite is in some respects rather trivial because the role of the RUM is self-evident. Indeed, for other examples the fact that both high- and low-symmetry structures can form with ideal tetrahedra provides a posteriori evidence that the phase transition between the two structures must involve condensation of a RUM. However, our analysis goes beyond this trivial a posteriori evidence because the simple prediction of a RUM soft mode is only part of the story. Often it is also important to know whether the RUM occurs at a single wave vector in reciprocal space, or whether the RUM is part of a line or plane of RUMs, as in perovskite. For example, issues such as the nature of the high-symmetry phase and the role of critical fluctuations (Sollich et al. 1994) both hinge on this aspect. This information cannot be deduced from a posteriori reasoning or any other means of reasoning. The factors determining the phase-transition temperature, and cation ordering, are other issues involving the concept of rigid-unit modes in nontrivial ways.

Some notes on the calculation of RUMs

The important computational approach in our work is the calculation of the rigid-unit mode spectrum for each structure of interest. We used the split-atom method of Giddy et al. (1993). The rigid tetrahedra are considered to be the independent molecules, and each O atom that is shared by two linked tetrahedra is considered to be two individual "atoms" separated by a distance of zero. To prevent the split atoms from separating, a strong harmonic force acts between them. The dynamical equations of this model are then solved using standard methods for the calculation of the phonon-dispersion curves for molecular crystals. The RUMs are calculated to be the normal modes in which the split atoms move together, and thus they have a calculated frequency of zero. The split-atom method has been programmed into a standard molecular lattice-dynamics program (Pawley 1972; Dove 1993). The method, and the resultant program called CRUSH, have been described in detail elsewhere (Giddy et al. 1993; Hammonds et al. 1994). Although the split-atom method may initially seem to be rather artificial, the split-atom force constant is formally identified with the stiffness of the tetrahedron (Dove et al. 1996a). We therefore chose a value for the split-atom force constant that reproduced the experimental range of phonon frequencies, excluding the highest energy Si-O stretching modes.

The split-atom model has been extended to include interactions between the centers of the tetrahedra, modeled as a harmonic energy that changes if the separation between the two centers changes (Hammonds et al. 1994). This can be interpreted physically as an attempt to maintain a constant Si-O-Si bond angle. RUMs that do not involve any change in this angle are described as "torsional modes," and this interaction is called the "torsional interaction."

In some cases our calculations were performed using structures with geometrically perfect tetrahedra, which were set up using a program called IDEALISER. Analysis of the results of a CRUSH calculation was performed using a second program, which includes an interface to

the group-theory program of Warren and Worlton (1974) for the assignment of mode symmetries to the RUMs. These two programs have been described by Hammonds et al. (1994) and together with the CRUSH program are available on the World Wide Web at http://www.esc.cam.ac.uk/mineral_sciences/crush.html.

In all our tabulations of RUMs we defined the wave vector with the use of the standard nomenclature for the special points in the Brillouin zones as used by Stokes and Hatch (1988)—points on the surface of the Brillouin zone are given by Roman letters, and inside the Brillouin zone by Greek letters—although in the tables the wave vectors are given explicitly. In general the symmetries of the RUMs are not specified to reduce the complexity of the tables, but the degeneracies of the modes are specified using the labels A for a single mode, E for a doubly degenerate mode, T for a triply degenerate mode, and F for a quadruply degenerate mode. When the symmetry of a mode is given, it is represented by the symbol for the wave vector, which defines the point symmetry of that wave vector, and a subscript label, which defines the irreducible representation of this point group. The labels are fully consistent with the usage of Stokes and Hatch (1988). For example, in β-quartz the wave vector at the center of the Brillouin zone is labeled Γ, and the modes at the zone center are labeled Γ_1–Γ_5. In other cases some of the irreducible representations are two- or three-dimensional, and to indicate this an appropriate superscript is added. For example, in the case of the cubic β-cristobalite, there are two two-dimensional modes at the (1,0,0) zone-boundary point, which are labeled $^2X_3$ and $^2X_4$. On the other hand, for modes at the zone center it is common to employ the spectroscopic notation, for example, A_{2g} or E_u. A consistent nomenclature is not used for symmetry, but for each material the conventions set by previous workers are followed.

Quasi-RUMs

We usually think of the phonon modes that are not RUMs as having reasonably high frequencies because the forces involved in distorting the SiO_4 tetrahedra are large. In the case of the optic modes in β-quartz at $\mathbf{k} = 0$, our split-atom calculations give a single RUM, two modes at $\sim$3 THz and a band of modes between 13 and 25 THz. There is, however, a continuum of frequencies from 0 THz upward when taking account of the modes at $\mathbf{k} \neq 0$ that are RUMs at special wave vectors because their frequencies increase for wave vectors away from their special positions. This, of course, is exactly as expected and does not lead to any important consequences.

By way of comparison, the range of the mode frequencies calculated for both β-cristobalite and high-tridymite at $\mathbf{k} = 0$ is 10–24 THz, using the same split-atom force constant. On the other hand, for cordierite the corresponding range is 0.6–26 THz, and for leucite it is 0.4–25 THz. For these relatively complicated crystal structures, containing several tens of tetrahedra in each unit cell, there is scope for some of the normal modes to involve just a relatively small amount of distortion. Indeed, for some wave vectors in these materials the frequencies can be considerably <1 THz. In these cases the distinction between RUMs and other modes becomes blurred. We call any such low-frequency mode a quasi-RUM, or QRUM. It should be noted that the value of ω^2 for any QRUM is a measure of the magnitude of the distortion of the tetrahedra caused by this vibration.

One might expect a structure to have more QRUMs if it is geometrically similar to some parent structure with greater symmetry, with more true RUMs. The frequencies of these QRUMs increase rapidly as the amplitude of the distortion relating the parent and daughter structures increases, such as when the temperature is lowered below a displacive phase transition. Also, such QRUMs are not usually scattered evenly over the Brillouin zone but occur in the lines and planes in reciprocal space that contain RUMs in the parent structure.

Quartz

The phase transitions in quartz

The stable polymorph of SiO_2 at ambient temperature and pressure is α-quartz, which has a trigonal structure with space group $P3_121$. At 846 K quartz undergoes a first-order phase transition to an incommensurate phase, and at only 1.5 K higher there is a second-order displacive phase transition to the hexagonal β phase, with space group $P6_222$ (Dolino 1990). Although the α-incommensurate phase transition is first order, the discontinuities in the crystal properties are small, and the order parameter has a temperature dependence that is close to that of a classical tricritical phase transition (Carpenter et al., in preparation). The incommensurate phase transition is caused by the softening of a phonon at the wave vector $\mathbf{k} \approx 0.05a^*$. These phase transitions were recently reviewed by Dolino (1990).

RUMs in the α and β phases of quartz

The complete set of RUMs for both the α and β phases of quartz are given in Table 1. The results for the β phase of quartz are in complete agreement with the results obtained by Vallade et al. (1992). However, we explicitly incorporate the zone-boundary points, which were not included in the results of Vallade et al. (1992). The RUMs in β-quartz that occur in planes of wave vectors in Table 1 are acoustic modes. The results for the α phase have not been given elsewhere.

The results of Table 1 for β-quartz have been confirmed by inelastic neutron-scattering experiments (Berge et al. 1986; Bethke et al. 1987; Dolino et al. 1992). The optic RUMs were found to be of low frequency along the lines in reciprocal space predicted in Table 1. On cooling toward the phase transition the lines of RUMs were found to soften almost uniformly.

The Γ_5 RUM of the β phase is the soft mode of the α-β phase transition, and its eigenvector is identical to the distortion found in the α phase (Giddy et al. 1993). The

TABLE 1. Rigid-unit modes for the hexagonal and trigonal structures

	β-quartz $P6_222$	α-quartz $P3_121$	Tridymite $P6_3/mmc$	Kalsilite $P6_3$	Nepheline $P6_3$	Cordierite $P6_3/mmc$
Γ (0,0,0)	A		2A + 2E	E	E	2A + 2E
A (0,0,½)	A + E	A	E + F	2E		E + F
H (⅓,⅓,½)	A	A	2A		E	
K (⅓,⅓,0)	A	A	A	A	2A + E	2A + 2E
L (½,0,½)	A	A	E			E
M (½,0,0)	2A	A	3A	A	4A	6A
Δ (0,0,ξ)	3A		2A + 2E	4A		2A + 2E
Λ (ξ,ξ,0)	A	A	A	A	4A	6A
Σ (ξ,0,0)	2A		3A			6A
Q (ξ,ξ,½)	A	A				
R (ξ,0,½)			E			
S (½ − ξ,2ξ,½)	A	A				
T (½ − ξ,2ξ,0)	A	A	A	A	4A	6A
U (½,0,ξ)	A		2A			6A
(ξ,ξ,0)	A		A	A	4A	6A
(ξ,0,ξ)			2A			

two Σ_2 RUMs along [1,0,0] are the transverse acoustic mode polarized along [0,0,1] and an optic mode with part of the second transverse acoustic mode (i.e., the x-y shear mode) mixed in. It is this mixed mode that becomes the Γ_5 RUM at $\mathbf{k} = 0$ and is involved in the incommensurate instability. The mechanism proposed by Vallade and coworkers (Berge et al. 1986; Vallade et al. 1992) involves an almost uniform softening of the mixed Σ_2 RUM for all wave vectors along the branch. At $\mathbf{k} \neq 0$ the Σ_2 RUM has the same symmetry as the pure transverse acoustic mode (the x-y shear mode). Because the RUM and the acoustic mode have the same symmetry they can interact, their eigenvectors mix, the frequency of the optic mode increases, and the frequency of the acoustic mode decreases. The effect on the mode frequencies is strongest for the wave vectors where the two modes have similar frequencies. Because the acoustic mode and the optic RUM have different symmetry at $\mathbf{k} = 0$, the interaction vanishes at this point and varies with $\mathbf{k}$ as k^2. The result is that as the Σ_2 optic RUM softens on cooling, it mixes with the acoustic mode and drives it soft at an incommensurate wave vector. The important point is that the incommensurate instability arises as a natural consequence of the existence of a line of RUMs. The interaction of a soft optic mode with an acoustic mode that varies as k^2 is reasonably common, but in most cases the optic mode softens only at a single wave vector, $\mathbf{k} = 0$, for example. Then, the interaction with the acoustic mode is not strong enough to lead to an incommensurate instability. In the case of quartz the existence of a line of RUMs leads automatically to the possibility of the incommensurate instability. This was documented in detail by Berge et al. (1986) and Vallade et al. (1992). This model has been tested by a molecular dynamics simulation study of the collective dynamics of the β phase of quartz (Tautz et al. 1991). By comparing the eigenvectors of the soft optic branch with the RUM eigenvectors it was found that the two matched to within 80%.

The comparison of the RUM results for the α and β phases of quartz shows that some of the modes are RUMs only in the higher symmetry β phase. This follows an empirical rule discussed by Giddy et al. (1993) that RUMs do not always commute, that is, when a structure is modulated by the imposition of one RUM, the subsequent loss of symmetry breaks some of the degeneracies of the constraints and causes some of the modes to cease being RUMs. This is because finite rotations (of the tetrahedra) do not simply add. From an experimental viewpoint the most interesting example of this is an M_2 mode. In the α phase this mode is observed to soften significantly on heating to the phase-transition temperature (Boysen et al. 1980). From Table 1 it is seen that this mode is a RUM in the β phase but not in the α phase (there are two M_2 modes in Table 1, the other of which remains a RUM in the α phase and was found experimentally not to vary strongly with temperature). Therefore, it has a moderately high frequency at low temperature in the α phase but softens as the temperature approaches the α-β phase transition where it becomes a RUM. We calculated the frequencies of all modes that are RUMs only in the β phase for different values of the order parameter Q using the rigid-unit mode program CRUSH. For all modes on special points and lines the frequency varies as $\omega^2 \propto Q^2$, whereas for the modes with wave vectors on a plane of symmetry $\omega^2 \propto Q^4$. Where $\omega^2 = \kappa Q^2$, the specific coefficients for the modes were placed on an absolute scale by using an appropriate value for the split-atom force constant and assuming that $Q = 1$ corresponds to the value at $T = 0$ (as given by our own neutron diffraction measurements, unpublished data), and these are given in Table 2. Aside from the soft mode at Γ, the most sensitive modes are the M_2 and A modes. The large shift in the frequency of the M_2 mode was determined by the inelastic neutron-scattering measurements of Boysen et al. (1980). From their data we estimated that experimentally the frequency of the M_2 mode (in THz^2) varies as $\omega^2 = 12Q^2$: The coefficient is in reasonable agreement with the value given in Table 2, particularly taking account of the gross approximations inherent in the split-atom calculations.

TABLE 2. Coefficients in the equation $\omega^2 = \alpha Q^2$ for the frequencies of modes that are RUMs in β-quartz but that have nonzero frequency in the α phase

Mode	α
Γ	16.6
Δ	1.4
Σ	0.4
A	9.4
M	10.4
U	9.2

Note: The unit for frequencies is THz, and Q is defined to equal 1 at 0 K.

The origin of the α-β phase transition in quartz

With many RUMs at different special points in the Brillouin zone, we must ask what factors determine which RUM will act as the soft mode to generate a new low-temperature phase. In theory there may not be a general answer to this question because phase transitions usually arise from a delicate balancing of different forces, and in a general case it might simply be that a given transition occurs when the balance tips a certain way. However, in the case of quartz the RUM model may give a more specific answer to this question.

The first thing to note is that there is always a force that acts to reduce the volume of the structure. The most obvious candidate force arises from the dispersive interactions between the highly polarizable O anions. If the lowest order interaction between two O atoms varies with the separation r as $-Ar^{-6}$, where A is a constant, the integration of this interaction over the whole crystal follows as

$$-\int_{r_0}^{\infty} Ar^{-6} \times 4\pi\rho r^2 dr = -\frac{4\pi\rho A}{3r_0^3}$$

where ρ is the density of O atoms, and r_0 is a lower cutoff. This energy is more negative for higher densities and therefore favors configurations with lower volumes. Because the β phase of quartz is fully expanded, any distortion to lower symmetry leads to a reduction in volume. The dispersive interaction is therefore a positive driving force for any of the potential RUM distortions. It is therefore likely that the RUM distortions that produce the largest volume changes are preferred over the other RUM distortions. We show elsewhere (Dove et al., in preparation) using lattice-energy calculations that the driving force from the dispersive interactions is certainly strong enough to account for the phase transition in quartz. The Coulomb interactions have been found to be much less significant in this respect.

In addition to the volume change acting as a general driving force for a phase transition, we also need to take account of local interactions. Apart from short-range steric forces, which eventually limit the extent to which the structure can distort to lower the volume, there is an energy associated with the distortion of the Si-O-Si bond. In systems such as cristobalite the relaxation of the crystal to produce bond angles in the ideal range 145–150° provides a driving force for the phase transition. On the other hand, in β-quartz the Si-O-Si bond is already in this range, and any RUM distortion that changes this angle substantially raises the energy. The way each RUM distorts or preserves the equilibrium Si-O-Si bond angle can be modeled by the torsional interaction. When this interaction is nonzero only the torsional RUMs retain their zero frequency. In β-quartz the only RUMs that have zero frequency with a nonzero torsional interaction are A modes at the Γ, A, and M points. The RUM with zero frequency at Γ is the Γ_5 RUM that acts as the soft mode for the α-β phase transition. The torsional interaction, therefore, selects a few RUMs from the complete set that might act as soft modes for displacive phase transitions. Although it is known that there is a systematic change in the Si-O-Si angle on cooling below the phase transition, the point is that this change is quadratic in the rotations of the tetrahedra rather than linear, as demonstrated by lattice calculations with rigid tetrahedra (unpublished data).

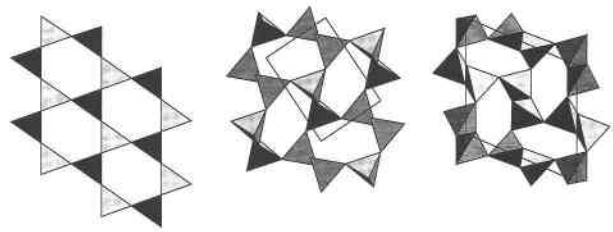

FIGURE 2. The three phases of cristobalite viewed down a common direction, [110] in the β phase and [010] in the α phase and the high-pressure phase II. The data for the structure of phase II were kindly provided by Larry Finger (1993, personal communication). The outlines of the unit cells are marked in the latter two cases.

CRISTOBALITE

The α-β phase transition in cristobalite

Cristobalite is another polymorph of silica containing corner-sharing SiO_4 tetrahedra. At atmospheric pressure it is stable only at temperatures above 1840 K, but it can be easily supercooled without reversion to quartz or tridymite. The high-temperature β phase has an idealized cubic structure of space group $Fd\bar{3}m$. At approximately 530 K (dependent on the sample quality) it undergoes a first-order phase transition to the tetragonal α phase with space group $P4_12_12$ (Schmahl et al. 1992). The transition is consistent with an unstable mode at the wave vector (1,0,0), the X point, and the symmetry change is consistent with this mode having symmetry X_4 (Hatch and Ghose 1991). The structures of the α and β phases are shown in Figure 2 as viewed from a common direction to illustrate the rotations and translations of the tetrahedra.

The α-β transition in cristobalite has recently been

studied in some detail using a variety of approaches. Hatch and Ghose (1991) presented the group theoretical basis for our understanding of this phase transition. Schmahl et al. (1992) presented new crystallographic data, which when merged with previous data led to the construction of the Landau free-energy function. Spearing et al. (1992) and Phillips et al. (1993) studied the phase transition with the use of nuclear magnetic resonance techniques. Swainson et al. (1996) studied the transition with the use of infrared and Raman spectroscopy. Swainson and Dove (1993a, 1995a) also reported molecular dynamics calculations and inelastic neutron-scattering results, which point to the existence of many low-frequency modes in the β phase. These modes were found to disappear on cooling into the α phase. Hua et al. (1988; see also Welberry et al. 1989 and Withers et al. 1989) reported the observation of strong diffuse electron scattering in the ⟨110⟩ zones of the β phase, which disappears in the low-temperature phase. Strong diffuse scattering has also been found in neutron powder diffraction results for the β phase (Schmahl et al. 1992), reminiscent of the diffuse scattering observed from orientationally disordered crystals (Dolling et al. 1979). Withers et al. (1989) suggested that the diffuse scattering at the X point can be explained in terms of coupled rotations of rigid tetrahedra in planes perpendicular to the ⟨110⟩ directions, that is, in effect, in terms of RUMs.

Despite all the work that has been conducted on cristobalite, there remains a fundamental controversy concerning the nature of the high-temperature β phase. Some authors, including Hatch and Ghose (1991), have proposed that the β phase consists of domains of the α phase with random orientations, so that the symmetry of the β phase is recovered as the macroscopic average over all domain orientations. A related model was proposed by Wright and Leadbetter (1975), but in this case the β phase is composed of domains of a different symmetry ($I\bar{4}2d$), and again the macroscopic symmetry of the β phase follows from the average over all domains. Although these models attract support from some authors (e.g., Spearing et al. 1992), the NMR data of Phillips et al. (1993), the spectroscopic data of Swainson et al. (1996), and the molecular dynamics simulations and inelastic neutron-scattering data (Swainson and Dove 1993a, 1995a) tend to support the opposite view that the β phase does not contain recognizable domains of any other structure. Because the idealized structure of the β phase is chemically implausible as a static structure—the Si-O bond lengths are significantly shorter than typically found in silicates, and the Si-O-Si bond is linear—it is clear that there must be a substantial amount of orientational disorder of the SiO_4 tetrahedra in the β phase. The controversy concerning the structure of the β phase, therefore, revolves around the issue of the scale of the correlations associated with the orientational disorder, in both space and time. In the domain models these correlations are long ranged, with a long lifetime (at least relative to phonon periods), whereas the interpretation of the NMR and spectroscopic data suggests that the correlations are both short ranged and of a short lifetime.

The β phase of cristobalite also undergoes a first-order phase transition on increasing pressure at ambient temperatures. The high-pressure phase, which Palmer and Finger (1994) labeled phase II, is monoclinic with space group $P2_1$. From the tables of Stokes and Hatch (1988) it is seen that the symmetry of phase II can be derived from that of the α phase by a distortion of wave vector (½,0,½). The phase transition is allowed to be second order, but on increasing pressure it is found to be strongly first order.

RUMs in the three phases of cristobalite

The RUM analysis of the two low-pressure phases of cristobalite is given in Tables 3 and 4. For the β phase we used the ideal structure in our calculations, although we noted above that this is chemically implausible as a static structure, the ideal structure represents the point from which the disordered phase is derived.

The RUM spectrum of the β phase of cristobalite (Dove et al. 1991; Swainson and Dove 1993a) is easily described as having one RUM for each wave vector in each of the ⟨110⟩ zones, that is, there are six whole planes of RUMs in reciprocal space. These planes of RUMs are clearly seen in the lattice-dynamics calculations of Dove et al. (1991, 1992). Two planes intersect at the X point, and the two corresponding RUMs form the doubly degenerate X_4 mode, which is the soft mode for the α-β phase transition (Hatch and Ghose 1991). Thus, as with the α-β phase transition in quartz, the RUM analysis yielded the soft mode for the phase transition, at least to the extent to which the instability in cristobalite is driven by a soft mode (this point was discussed by Swainson et al. (1996), who reported the existence of well-defined soft modes in the α phase).

The RUMs in the β phase of cristobalite received experimental confirmation from two studies. First, these RUMs have been observed as strong streaks of diffuse scattering in electron diffraction measurements. Measurements performed in different zones, and by tilting the sample to observe out-of-plane scattering, have confirmed all details of the results given in Table 3. In the classical limit, the intensity of diffuse scattering from a phonon scales as ω^{-2}, where ω is the angular frequency of the phonon (Dove 1993). Thus, the most intense features of diffuse scattering come from low-frequency phonons, and because RUMs are expected to be the lowest frequency modes in a structure it should be possible to relate the diffuse scattering to the RUM spectrum. Indeed, as we have noted, all the streaks of diffuse scattering in β-cristobalite can be accounted for as single-phonon scattering from RUMs. The streaks themselves are relatively narrow in wave vector and appear to be no wider than the resolution of the measurements. We comment on this below. Second, the many low-frequency modes in β-cristobalite have been observed in a measurement of the phonon density of states (Swainson and Dove 1993a,

TABLE 3. Rigid-unit modes for the cubic structures

	β-cristobalite *Fd3m*	Sodalite *Im3̄m*	Sodalite *I4̄3m*	Sodalite *P4̄3n*	Leucite *Ia3d*
Γ (0,0,0)	T	A + T		T	2A + T
L (½,½,½)	A + E				
X (0,1,0)	E				
H (0,0,1)		T	T		
N (½,½,0)		3A	2A		2E
P (½,½,½)		3A	A + E		
X (0,0,½)				F	
M (½,½,0)				2E	
R (½,½,½)				E + F	
Δ (ξ,0,0)	E	A + E	E	2E	
Λ (ξ,ξ,ξ)	A + E	A	A		
Σ (ξ,ξ,0)	A	A + E	A		4A
S (ξ,ξ,1)	A				
R (ξ,0,½)					
D (½,½,ξ)		2A	2A	2E	
F (ξ,1 − ξ,ξ)		A	A		
G (ξ,1 − ξ,0)		2A	A		
(ξ,ξ,ζ)	A		A		
(ξ,ζ,0)		2A			
(ξ,ζ,λ)		A			

TABLE 4. Rigid-unit modes for the tetragonal and orthorhombic structures

	α-cristobalite $P4_12_12$	Leucite $I4_1/acd$	Cordierite *Cccm*
Γ (0,0,0)	A	3A	6A
M (½,½,0)	E		
X (½,½,0)		2E	
Y (1,0,0)			6A
Z (0,0,½)			3E
S (½,½,0)			6A
T (1,0,½)			E
R (½,½,½)			2A
Σ (ξ,ξ,0)	2A		
Δ (ξ,ξ,0)		4A	
Σ (ξ,0,0)			6A
Δ (0,ξ,0)			6A
Λ (0,0,ξ)			6A
H (1,0,ξ)			2A
F (1,ξ,0)			6A
(ξ,ζ,0)			6A

1995a), where a striking difference was noted between the α and β phases (see below). These density-of-states measurements were consistent with the prediction from molecular dynamics simulation (Swainson and Dove 1995a). Comparison of the inelastic neutron-scattering experiments on the β and α phases of cristobalite gives the energy scale for the RUMs of about 0–1 THz. This is consistent with inelastic neutron-scattering results for leucite (Boysen 1990), which are discussed later.

The comparison of the RUM spectrum of the α phase of cristobalite with that of the β phase is striking. Virtually the only RUMs that remain in the α phase lie in the [110] direction, and there are no longer whole planes of RUMs. Not included in the table is the existence of a curved line of RUMs. The difference between the number of RUMs in the two phases was clearly seen in the measurements of the phonon density of states by inelastic neutron scattering (Swainson and Dove 1993a). The results confirmed that there are many fewer low-frequency modes in the α phase. Moreover, the electron diffraction results also show the sudden changes in the RUM spectrum on cooling below the transition temperature (Hua et al. 1988).

Finally, our analysis of cristobalite II shows that it has no RUMs for any of the symmetry points or directions in the Brillouin zone. The crystal structure has not yet been reported, but preliminary details were given to us by Larry Finger (1993, personal communication). Our CRUSH calculations were performed on a structure that was idealized to have perfect tetrahedra, which is shown in Figure 2.

RUMs and the nature of the β phase of cristobalite

So far we have seen how RUMs can provide the instabilities associated with phase transitions. In the case of cristobalite they are also essential in determining the nature of the high-temperature phase. As noted above, the evidence from experiments (Schmahl et al. 1992; Swainson and Dove 1993a, 1995a; Swainson et al. 1996) and simulations (Swainson and Dove 1993a, 1995a) indicates a high degree of disorder in the β phase. The Si-O bonds rotate away from the ⟨111⟩ directions, so the Si-O-Si bond angles are approximately 140–150° (Swainson and Dove 1995b). If the tetrahedra are to remain rigid, they must rotate by about 15–20°. If the RUMs were restricted only to lines of wave vectors in reciprocal space this would not be easily accomplished. However, in β-cristobalite there are planes of RUMs, and the disorder can be achieved as a superposition of all RUMs.

We illustrate this by showing how the two domain models of β-cristobalite, from Hatch and Ghose (1991) and Wright and Leadbetter (1975), can be explained in terms of RUMs. The model of Hatch and Ghose (1991) supposes the existence of slowly fluctuating domains of the α phase. We consider one such domain with the tetragonal axis along [0,0,1], say, as a local wave packet made by superposing phonon modes near the X point in reciprocal space, (0,0,1), using, of course, the phonon bands that run into the X_4 mode at X. If the domain has a platelet shape, it will involve phonon modes predominantly along and very near the RUM line $\mathbf{k} = (0,0,k_z)$ near (0,0,1). If, on the other hand, it has a rod shape along [1,1,0] or [1,1̄,0] it will consist predominantly of modes in the (1,1,0) or (1,1̄,0) RUM planes. Either way the structure can be generated as a patchwork of wave packets of the three ${}^2X_4$ modes slowly fluctuating in time and space. Because everywhere the tetrahedra are locally rotated, there is a volume reduction analogous to that in Figure 1. The analysis can be carried two steps further. Because there is a tetragonal strain involved in the local region of the α domain, there is something like a domain boundary between, say, a region of $3z^2 - r^2$ strain and one with $3x^2 - r^2$ strain. The theory of coherent domain packets (Sapriel 1975) shows that the strain energy is minimized if the boundaries lie perpendicular to the [1,±1,0] axes. Thus, we predict that the domains are platelets perpendicular to these directions and not rod

shaped. The second point is that the relevant RUMs extend over the whole of the $(1,\pm1,0)$ planes, so there would appear to be no energy gain by making large coherent domains involving only the RUMs near X. We therefore predict for entropy reasons that the domains are very small, almost at the level of a unit cell. The model of Wright and Leadbetter (1975) proposes that the β phase is composed of domains of cubic $I\bar{4}2d$ symmetry, caused by condensation of the Γ_5^- (T_{2u}) RUM. Considerations similar to those outlined for the X_4 domains also apply in this case. However, the important point concerning both models is that the X_4 and Γ_5^- RUMs lie in the same planes of RUMs in reciprocal space (Swainson and Dove 1993b). Therefore, because either type of domain forms from wave packets of RUMs along the line from Γ to X, the wave packet that forms the X_4 domain automatically includes some of the Γ_5^- RUM, and vice versa. So there is no incompatibility between the two domain models, and indeed both are part of a larger model that allows domains formed from wave packets centered on any wave vector in the RUM planes, with domain sizes that can be as small as one unit cell and with low-energy domain walls. Exactly how the energy is partitioned between different types of domains is an experimental question.

Our picture of the β phase of cristobalite being disordered as a result of the action of many RUMs suggests that the phonons are strongly anharmonic. This would mean that if the diffuse scattering from a RUM could be analyzed in terms of its energy dependence (the sort of thing that is routinely done in an inelastic neutron-scattering experiment), the RUM phonon would not appear as a peak of single frequency but as a damped mode with a spread of frequencies. This damping could be no more than a broadening of the phonon peak (underdamping), or it could lead to the peak being completely replaced by a broad distribution of energies that encompasses both zero energy and the nominal harmonic energy of the phonon (overdamping). The latter situation is quite typical where there is strong orientational disorder of molecules or molecular units, as, for example, in SF_6 (Dove et al. 1986). The interesting point with respect to the diffuse electron scattering is that a shift in the energy distribution to lower frequencies leads to an increase in the intensity of scattering following the ω^{-2} scattering law (Dove 1993). This may explain why the streaks of diffuse scattering are so strong in the electron diffraction images. It may also help to explain why the streaks are so narrow in wave vector. Consider a point in reciprocal space on one of the streaks of diffuse scattering, and denote $\mathbf{q}$ as a vector normal to that point. The frequency of the phonon surface that contains both the RUM at our point on the streak and the phonon at $\mathbf{q}$ varies as $\omega^2(\mathbf{q}) = \omega_{\mathrm{RUM}}^2 + \alpha|\mathbf{q}|^2$, where ω_{RUM} is the harmonic frequency of the RUM at our point on the streak. We showed elsewhere that the coefficient α is related to the stiffness of the tetrahedron (Dove et al. 1992). In principle the width of the streak of diffuse scattering should give direct information about the magnitude of α. However, from our knowledge of the likely sizes of both ω_{RUM} and α it seems that the streaks of diffuse scattering are narrower than one would expect. This is possible if the RUM is heavily damped (or overdamped), with the distribution of energies being lowered by the damping. This point is illustrated in Figure 3. The damping is confined to the wave vectors close to the RUM planes, leading to an enhancement of the intensity of the diffuse scattering from the RUMs relative to that from phonons on the same branch.

The high-pressure α-II phase transition in cristobalite

We noted above that the α-II phase transition in cristobalite can arise as a result of a soft-mode distortion involving a phonon in the α phase with wave vector $(\frac{1}{2},0,\frac{1}{2})$. However, no RUM occurs in the α phase at this wave vector (Table 4). This might imply that the α-II phase transition does not involve RUM distortion. However, it is possible to generate the structure of phase II with perfect SiO_4 tetrahedra, which implies that a RUM distortion of some kind must be involved in the phase transition. Phase II can be derived from the β phase by a distortion with wave vector $(\frac{1}{2},\frac{1}{2},\frac{1}{4})$, and a RUM with this wave vector in the β phase lies on the planes listed in Table 3. Thus, we propose that phase II is not directly obtained from the α phase but instead is a distortion of the β phase, and that it is, indeed, one of the possible ordered structures that can be generated from the β phase. When cristobalite, therefore, transforms from the α phase to phase II, it must overcome a free-energy (potential energy) barrier, which is why the transition is first-order. To some extent this idea is counterintuitive if we compare this behavior with what happens on changing temperature at ambient pressure, certainly in the sense of the formalism of a Landau free-energy function in which only one coefficient is allowed to be temperature dependent. Although this behavior is expected when the Landau free-energy function is obtained from renormalized phonon theory (Dove et al. 1992; Dove 1993), there are no grounds at all for assuming that any of the coefficients are independent of pressure. Indeed, it is to be expected that all the coefficients are strongly affected by pressure, and it would not be surprising if the minimum of the free energy could shift from one distortion of the β phase to another on changing pressure. We postulate that this happens at the α-II phase transition in cristobalite, in which case the β phase is the parent structure of both the α and II phases, rather than the α phase acting as a parent phase for phase II. The comparison of the structures of the three phases in Figure 2 suggests a close relationship between the α phase and phase II, which arises because they are both derived from the β phase by the same RUM phonon branch. The difference is in the wave vector of the distortion, not in the mode of deformation.

RUMs, entropy, and reconstructive phase transitions in silica

To conclude our analysis of cristobalite, we compare the results for cristobalite with those of quartz to make a

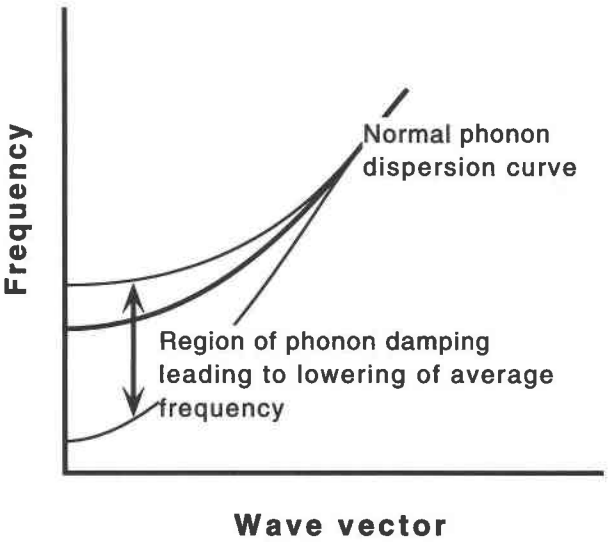

FIGURE 3. Diagram showing the spread of frequencies in cristobalite. For a wave vector for which the mode is not a RUM, the vibrations are harmonic and there is a tiny spread of frequencies. Close to the wave vector where the mode is a RUM, the mode is damped with a wider spread of frequencies, as marked by the vertical arrow, and the average frequency is lowered. Hence, the average value of ω^{-2}, which determines the intensity of one-phonon scattering, is enhanced by the damping at the RUM wave vector.

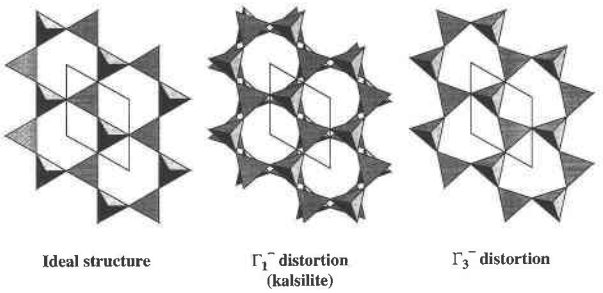

FIGURE 4. Structure of the ideal phase of tridymite (**left**), the derivative formed by condensation of the Γ_1^- RUM (**center**), which is equivalent to the highest symmetry kalsilite structure, and the derivative formed by condensation of the Γ_3^- RUM (**right**) leading to a structure with D rings. Each structure is viewed down the common [001] direction. The outlines of the unit cells are marked in each case.

qualitative point about the relative stabilities of quartz and cristobalite as a function of temperature. The energy of quartz must be lower than that of cristobalite because quartz is the stable phase of SiO_2 at low temperatures. For the reconstructive phase transition quartz-cristobalite to occur, the entropy must be greater in cristobalite than in quartz. The transition temperature at ambient pressures is high enough that we need to consider only the high-symmetry phases of both polymorphs. The rigid-unit modes as low-frequency modes carry a significant component of the entropy. In quartz there is a single plane of RUMs in reciprocal space, whereas in cristobalite there are six planes. Although the RUMs are strictly limited to these planes, the phonon branches that contain the RUMs have low frequencies in the vicinities of the RUM planes and therefore also contribute to the high phonon entropy. Thus, we can consider the RUM planes to have a finite effective thickness in reciprocal space, so that we can quantify the entropy contribution from the planes of RUMs by defining the ratio of the number of RUM planes to the number of tetrahedra in the unit cell. This ratio is $\frac{1}{3}$ for quartz and $\frac{6}{2} = 3$ for cristobalite. This simple comparison of the number of RUMs in both structures provides a mechanism (or at least part of the mechanism) for the entropy difference that allows the reconstructive phase transition to occur. We will see immediately below that a third polymorph of SiO_2, tridymite, has one plane of RUMs with one RUM and three planes of doubly degenerate RUMs. Because there are four tetrahedra in the unit cell, the ratio of the number of RUM planes to the number of tetrahedra is $\frac{1}{4}$, which is intermediate between quartz and cristobalite and consistent with the occurrence of tridymite between quartz and cristobalite in the SiO_2 phase diagram.

TRIDYMITE AND THE KALSILITE-NEPHELINE SOLID SOLUTION

The structure of tridymite and related materials

Tridymite is a third polymorph of silica and is stable between about 1030 and 1740 K. Its structure consists of sheets of corner-linked tetrahedra stacked perpendicular to the *c* axis, with the structure repeated every other layer. A single layer is shown in Figure 4. Although this structural arrangement is generally known, it is useful to compare it with cristobalite. The same sheets are found as (111) planes in cristobalite, but the stacking is different and repeats every third layer. The tridymite framework is the parent of a wide family of "stuffed" derivatives such as nepheline ($Na_3KAl_4Si_4O_{16}$) and kalsilite ($KAlSiO_4$).

RUMs in the ideal tridymite structure

The results of the RUM analysis of the ideal high-temperature tridymite framework, space group $P6_3/mmc$, are given in Table 1. As in β-cristobalite there are planes of RUMs in reciprocal space, although the RUM planes in tridymite are not all related to the RUM planes in cristobalite. There are more RUMs for the special wave vectors than in either quartz or cristobalite, which is due only in part to the fact there are more rigid units per unit cell and hence more phonon branches. The large number of RUMs in part accounts for the fact that tridymite is the parent to such a rich variety of daughter structures with varying compositions. The tridymite structure can adjust its geometry easily when cations of different sizes are introduced into its structure.

The results of the RUM analysis for high-tridymite given in Table 1 have been confirmed by recent electron

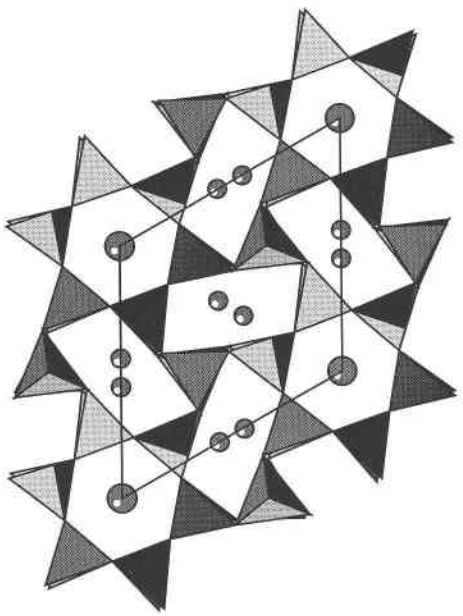

FIGURE 5. Crystal structure of nepheline viewed down the [001] direction. By comparison with Figure 4 it can be seen that the nepheline framework can be derived from the ideal tridymite framework by condensation of a zone-boundary RUM. The small spheres represent Na atoms and the large spheres represent K atoms. The structure has selected the RUM distortion that best holds the cations of two sizes. The outline of the unit cell is marked.

diffraction experiments (Withers et al. 1994). The RUMs appear as narrow streaks of diffuse scattering in the electron diffraction photographs, exactly as for β-cristobalite. We demonstrated elsewhere (Dove et al. 1996b) that these streaks can be explained by the calculated RUM spectrum given in Table 1. Because the same linear Si-O-Si bonds in the idealized tridymite structure are in the idealized structure of β-cristobalite, the same arguments developed for the disordered nature of the structure and the damping of the RUMs of β-cristobalite also apply directly to high-tridymite. The diffuse scattering seen by electron diffraction also shows a curved surface of diffuse scattering (Withers et al. 1994) that is not indicated by the results of Table 1. This also can be explained with the RUM model (Dove et al. 1996b). We were able to calculate an identical curved surface of RUMs that passes through points of special symmetry but which itself was not defined by symmetry. This is a significant point. In most cases surfaces of RUMs are planes of special wave vectors. Indeed, prior to these calculations we had anticipated that, because the number of RUMs is small in comparison with the total number of phonon modes, the RUMs would be restricted to special wave vectors as a general principle. Instead, there is nothing special about the wave vectors on the calculated curved surface in tridymite, which indicates that these sorts of features may be quite common. Indeed, we found other examples of general RUM surfaces, which are reported elsewhere.

RUM distortions of the ideal tridymite structure

The distortion of the high-temperature tridymite framework upon decreasing temperature is not well understood. Many different structures and space groups have been observed, as detailed in the reviews of Merlino (1984) and Wennemer and Thompson (1984). It is likely that many of the observed distortions of the high-temperature framework can be understood in terms of RUMs. For example, consider the structures produced from high-tridymite by the condensation of the two nondegenerate RUMs (labeled A in Table 1) at the zone center. Figure 4 shows a structure with a symmetry of $P6_322$ produced by the condensation of the RUM of symmetry Γ_1^- (A_{1u}). This framework is observed in kalsilite (Merlino 1984; Andou and Kawahara 1984). Figure 4 also shows the distortion produced by the RUM of symmetry Γ_3^- (B_{1u}): This is the distortion to D rings discussed by Wennemer and Thompson (1984). The two doubly degenerate RUMs at Γ have symmetry $^2\Gamma_5^-$ and $^2\Gamma_6^-$ (E_{1u} and E_{2u}). The actual distortions resulting from the condensation of these modes are in general a linear combination of their two components. Both of these doubly degenerate modes can produce daughter structures with orthorhombic symmetry ($C222_1$ and $Cmc2_1$ are both possible space groups) as observed in tridymite derivatives (Dollase 1967; Kihara 1978; Capobianco and Carpenter 1989). On the other hand, these modes can also lead to lower symmetry structures, as listed by Stokes and Hatch (1988). Some of these lower-symmetry structures have been reported in the literature (e.g., Kihara 1978).

The kalsilite-nepheline solid solution

In the kalsilite-nepheline solid solution there is a new role for RUMs, that of providing the mechanism for static distortions of the ideal parent structure to facilitate Na^+-K^+ cation ordering. This role has importance in the discussion below on sodalite and zeolites. Cations like to be surrounded by O anions. Moreover, the O anions like to be at a specific radius as given by the ionic radii. It would be energetically unfavorable to bring about such a situation through significant distortion of the SiO_4 and AlO_4 tetrahedra.

This is illustrated most simply by the kalsilite structure, which is shown as one of the distorted tridymite structures in Figure 4. To reduce the K-O distance the tetrahedra rotate about [001]. The distortion required to achieve this is the Γ_1^- RUM given in Table 1. The nepheline structure, which must accommodate both Na^+ and K^+ cations with a 3:1 ratio, is necessarily more complicated. This is shown in Figure 5. There is a particular RUM, the M_2^+ mode in Table 1, that can generate the ordered nepheline structure from the ideal tridymite structure. This RUM distortion brings about the required O displacements, leaving a large hexagonal hole for the K^+ cations and squeezed elongated holes for the Na^+ cations. The Na-O distance is self-regulating: The RUM displacement pattern can have any amplitude and adjusts itself to bring the Na-O separation to its optimum value.

Intermediate between the kalsilite and nepheline endmembers are two other phases, trikalsilite and tetrakalsilite (see, for example, Putnis 1992). These have the larger supercells of the underlying tridymite structure and incorporate deformations of individual six-membered rings that are similar to those found in both kalsilite and nepheline.

RUMs in kalsilite and nepheline

As noted, the structures of kalsilite and nepheline are produced by deformation of the ideal tridymite structure. The RUM spectra of these two structures are given in Table 1. There are fewer RUMs in these two phases than in the ideal tridymite structure. The structure of kalsilite still has ideal Si-O-Si bond angles of 180°, and we therefore expect again to find a disordered structure obtained by the operations of the complete set of RUMs. Both kalsilite and nepheline undergo displacive phase transitions on cooling from high temperatures, but the details are complicated and not unambiguous, and a complete RUM description takes us beyond the scope of the present article.

Feldspar

The feldspar family of structures

The feldspar family is a large and important group of minerals displaying very diverse and complex subsolidus behaviors. The feldspars with the highest observed symmetry are potassium feldspar (high-sanidine), high-temperature sodium feldspar (monalbite), and rubidium feldspar. These are all monoclinic with space group $C2/m$. The framework topology without interstitial cations is shown in Figure 6. The topology is based on connected four-membered rings of tetrahedra. In Figure 6 the idealized individual rings, before being joined to other rings, have point symmetry $\bar{4}2m$ (D_{2d}), and as a result the unit-cell angle β has the ideal value of 120°. However, the four-membered rings can distort without requiring any change of the space group symmetry of the structure, as in the sanidine structure (also shown in Fig. 6). The individual four-membered rings of tetrahedra now have point symmetry 2 (C_2), and the unit-cell angle β has a value lower than 120°. Megaw (1973) noted that these distortions of the rings can occur without any distortions of the tetrahedra; the tetrahedra simply rotate. We show below that this distortion in sanidine is given by a RUM with Γ_1 (or A_{1g}) symmetry.

Feldspars undergo several phase transitions as a function of temperature, pressure, and chemical composition (Carpenter 1988; Salje 1990; Putnis 1992). The alkali feldspars of composition $RAlSi_3O_8$, where R is a monovalent alkali cation such as Na^+, K^+, or Rb^+, undergo two coupled transitions, which both act to change the symmetry from monoclinic $C2/m$ to triclinic $C\bar{1}$ (Salje 1985). In albite, $NaAlSi_3O_8$, the first transition that occurs on cooling is a displacive transition, and the symmetry change is consistent with the transition being a proper ferroelastic transition driven by a soft acoustic mode. The second transition that occurs on further cooling involves Al-Si ordering. The transition temperature for Al-Si ordering does not change drastically on substitution of Na^+ by K^+ (Carpenter 1988). On the other hand, the transition temperature for the displacive phase transition decreases rapidly with increasing K^+ content, and for K^+ contents larger than about 25% the Al-Si–ordering transition occurs at higher temperatures than the displacive phase transition (Carpenter 1988).

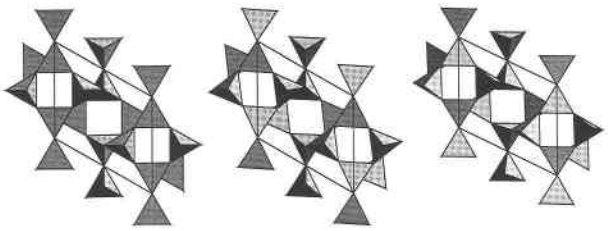

Figure 6. Three structures of feldspar with space group $C2/m$. The ideal structure (**left**) has the tetrahedra aligned to give rings of perfect fourfold symmetry and $\beta = 120°$. The intermediate structure (**center**) has rotated tetrahedra as a result of the condensation of the Γ_1 but still has $\beta = 120°$. The sanidine structure (**right**) is derived from the intermediate structure by a simple shear that does not change the symmetry. The outlines of the unit cells are marked in each case.

With feldspars of composition $MAl_2Si_2O_8$, where M is a divalent cation such as Ca^{2+}, Sr^{2+}, or Ba^{2+}, the Al-Si–ordering phase transitions are expected to occur at temperatures that are far higher than the melting temperatures. The Sr^{2+} and Ba^{2+} feldspars have the highest observed symmetry for this group: $I2/c$. There are two displacive transitions, which sequentially lead to the space groups $I\bar{1}$ (McGuinn and Redfern 1994a, 1994b) and $P\bar{1}$ (Redfern and Salje 1987, 1992; Redfern et al. 1988). The symmetry change $I2/c$ to $I\bar{1}$ is, as for the alkali feldspars, consistent with a proper ferroelastic instability. This is the phase-transition pathway followed by the Sr^{2+} and (possibly) Ba^{2+} members of this sequence. Calcium feldspar, $CaAl_2Si_2O_8$ (anorthite), is never observed in the $I2/c$ structure; the $I2/c$-$I\bar{1}$ transition is above the melting point (Carpenter 1988). The second displacive phase transition of $I\bar{1}$-$P\bar{1}$ is a zone-boundary transition (the unit cell doubles in size) and is observed only in anorthite and Ca-rich feldspars at relatively low pressures and temperatures (Redfern and Salje 1987, 1992; Redfern et al. 1988).

RUMs in the ideal and high-sanidine $C2/m$ structures

The RUM analysis for both the ideal ($\beta = 120°$) and real high-sanidine ($\beta \neq 120°$) structures is given in Table 5. The first point to note is that the ideal structure possesses more RUMs than high-sanidine, showing that the precise geometry can have a significant effect. For example, there are planes of RUMs in the ideal structure that are not found in the sanidine structure. The second point to note is the existence of a Γ_1 optic RUM at the

TABLE 5. Rigid-unit modes for the feldspar structures

	Ideal *C2/m*	Sanidine *C2/m*
Γ (0,0,0)	A	
Y (0,1,0)	2A	A
A (0,0,½)	A	A
M (0,1,½)	A	A
L (½,½,½)	2A	
V (½,½,0)	2A	
Λ (0,ξ,0)	2A	A
U (0,ξ,½)	A	A
(ξ,ξ,0)	2A	
(ξ,ξ,½)	A	
(ξ,0,ζ)	A	A

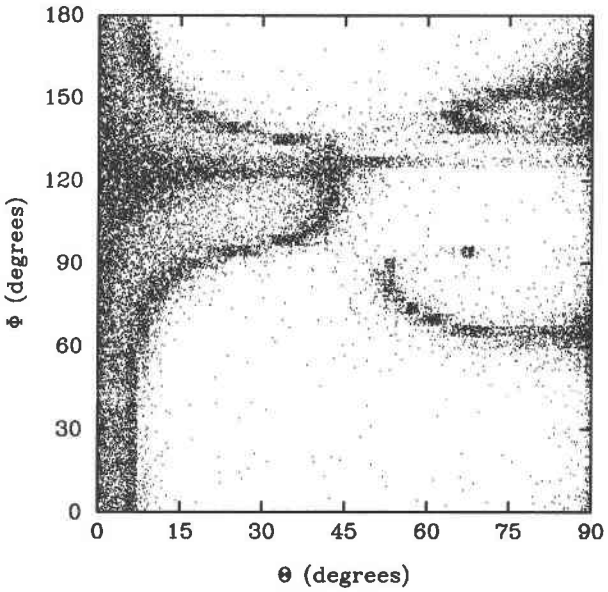

FIGURE 7. Contour map, represented as a polar plot, of the function $\Sigma\ 1/(\omega^2 + \Omega^2)$ obtained from CRUSH calculations, evaluated by summing all modes for each wave vector represented by the polar angles and with a fixed distance from $\mathbf{k} = 0$. The polar coordinates are defined such that θ gives the angle between $\mathbf{k}$ and b^*, and ϕ is the angle between the projection of $\mathbf{k}$ on the a^*-c^* plane and a^*.

zone center. This mode is totally symmetric in that its eigenvector does not destroy any of the space group symmetry elements. The eigenvector of this mode can be imposed onto the ideal structure to give a new structure that is also monoclinic with $\beta = 120°$ but somewhat deformed, as shown in Figure 6. This new structure is intermediate between the ideal structure and high-sanidine. Calculations showed that the intermediate structure has the same RUM spectrum as high-sanidine. The observed sanidine structure, with lattice parameter $\beta = 116°$, can be derived from the intermediate structure by an appropriate shear strain. This shear is again totally symmetric and is given by the transverse acoustic RUMs with wave vectors and polarization in the a^*-c^* plane.

The *C2/m*-*C*$\bar{1}$ ferroelastic phase transition in albite

The monoclinic-triclinic displacive instability that produces a phase transition in albite at ~1250 K generates no change in the size of the unit cell, which implies that the instability occurs at $\mathbf{k} = 0$. The point-symmetry change, $2/m \rightarrow \bar{1}$, is consistent with a ferroelastic instability but also allows an optical instability of the same symmetry. In this latter case, the optic instability couples linearly with the appropriate strain, leading to a shear of the unit cell that varies linearly with the order parameter. If the phase transition is a true ferroelastic transition, the strain is the order parameter, and any thermodynamic model (such as Landau theory) should be formulated without any additional optical instability. On the other hand, if there is an optical instability, the thermodynamic models can be formulated in such a way that simply brings in a linear coupling to strain. In the case of Landau theory, the issue is whether, as in the ferroelastic case, the $T - T_c$ prefactor should come in the strain term or in the terms containing a general order parameter, with only a constant prefactor in the pure strain terms. From Table 5 it is seen that there are no optic RUMs in sanidine at $\mathbf{k} = 0$. There are, however, three acoustic RUMs for wave vectors in some directions in the Brillouin zone. This is illustrated in Figure 7, which shows a contour map of the magnitude of the sum $\Sigma\ 1/(\omega^2 + \Omega^2)$ calculated for sanidine by the CRUSH program for each wave vector in the plot, which is actually shown as a polar plot for fixed magnitude of the wave vector $|\mathbf{k}|$ and therefore gives information about the soft directions of the acoustic modes. In this case Ω is a small constant chosen to avoid divergence when $\omega = 0$, and the summation is over all modes for each $\mathbf{k}$. The most significant components of this sum come from the acoustic modes with small values of $\partial\omega/\partial|\mathbf{k}|$, including the acoustic RUMs. From this plot we note that the soft acoustic modes lie along [0,1,0] and for all wave vectors in the a^*-c^* plane. Figure 8 shows the three acoustic modes for the directions a^*, b^*, and c^* calculated from CRUSH. There is an acoustic RUM with zero frequency for all wave vectors along each of these directions, and all the other acoustic modes have zero gradient at $\mathbf{k} = 0$, so that acoustic mode frequencies vary as $\omega \propto k^2$ in the limit $\mathbf{k} \rightarrow 0$. The existence of three soft acoustic modes along each direction implies that the feldspar framework can be sheared in any direction or even uniformly compressed in a concertina-like fashion. In reality interunit forces ensure that the elastic constants are nonzero, but because interunit forces are much smaller than intraunit forces, the elastic constants in feldspars are predicted to be small.

In the specific case of the monoclinic-triclinic phase transition, the crystal must become unstable with respect to a particular shear when the combination of elastic constants $C_{44}C_{66} - C_{46}^2$ falls to zero (Cowley 1976). Although the rigid-unit model indicates that all three of the acoustic modes for the feldspar framework are soft at the Γ point, the important modes are probably the acoustic RUMs. The plane of acoustic RUMs requires that both C_{44} and

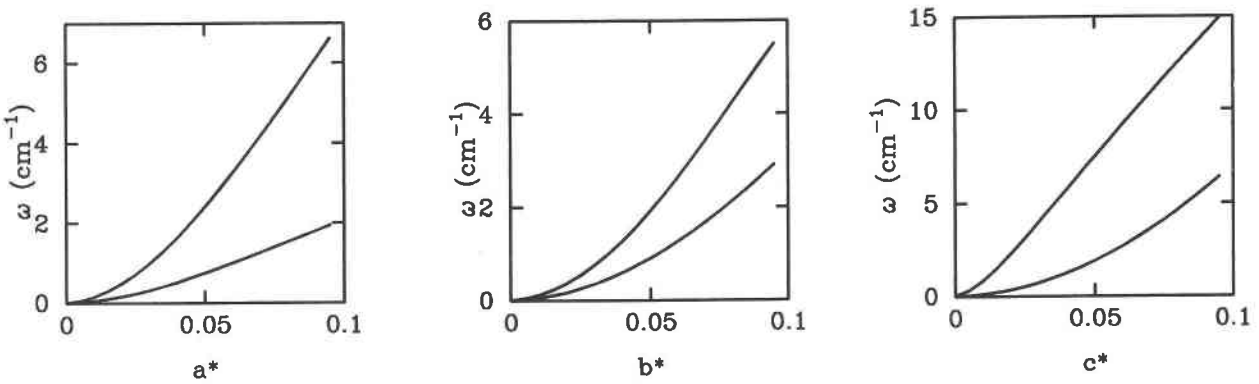

FIGURE 8. Soft acoustic modes along a^*, b^*, and c^* for sanidine calculated using CRUSH.

C_{66} be soft, although the stability condition does not require that either actually vanishes at the phase transition. That both elastic constants are naturally soft implies that the stability condition can easily be met, precipitating the observed ferroelastic phase transition. This basic picture has been confirmed by lattice calculations (Dove and Redfern 1997).

The $I2/c$-$I\bar{1}$ ferroelastic phase transition in $SrAl_2Si_2O_8$

The $I2/c$-$I\bar{1}$ transition occurs when the composition of the strontium feldspar $SrAl_2Si_2O_8$ is varied toward the Ca end-member, anorthite (McGuinn and Redfern 1994a, 1994b). The RUM spectrum calculated from the experimentally determined and idealized structures of both strontium and barium feldspars indicates that there are no optic RUMs in the $I2/c$ phase, but QRUMs replace some of the RUMs found in the ideal or sanidine phases (Table 5). Thus, the transition is caused by a soft acoustic mode of the type that causes the ferroelastic $C2/m$-to-$C\bar{1}$ phase transition in albite, and the CRUSH calculations indicate that the acoustic modes have the same sort of softening as in albite. In effect, the discussion of the ferroelastic phase transition in albite can be applied directly to the present case. Experiments also indicate that with a certain amount of Al-Si disorder the $I2/c$-$I\bar{1}$ phase boundary is shifted toward the anorthite end (Tribaudino et al. 1993), i.e., more of the smaller Ca^{2+} ions must be present to allow the framework to collapse at the same temperature. This shows the effect of Al-Si disorder hardening the soft acoustic modes and moving the transition point to more extreme conditions. This has been confirmed by lattice calculations (Dove and Redfern 1997).

The $I\bar{1}$-$P\bar{1}$ phase transition in anorthite

The $I\bar{1}$-$P\bar{1}$ phase transition in anorthite involves a doubling of the unit-cell size and therefore involves an instability with a wave vector on the Brillouin zone boundary. X-ray diffraction patterns indicate that there are two critical points on the Brillouin zone boundary, labeled Z and Z' (Salje 1985, 1987). There has been some discussion over whether the transition can be described as a simple displacive phase transition with the (by now) usual distortions of the framework of $(Si,Al)O_4$ tetrahedra, or whether the transition is in some way driven by ordering of the Ca^{2+} cations in their cavity sites.

Calculations performed with CRUSH for structure obtained from an X-ray structure refinement did not indicate the presence of a RUM at either of the critical points; indeed, as with the $I2/c$ phase, no optic RUMs were calculated at any wave vector. However, we were able to generate a structure with RUMs at these points by making very small modifications to the experimental structure. This was obtained by idealizing the tetrahedra and then very slightly (i.e., by $<0.1\%$) modifying the unit-cell parameters. This latter step is equivalent to adding small strains to the crystal structure, and it points to the important coupling between strain and the displacive phase transition. We found that the existence of a RUM at the Z point, (0,0,1), could be obtained for a range of strain distortions rather than for a single structure.

The coupling between strain and the lattice instability in the $I\bar{1}$ phase of anorthite is possibly important for two reasons. First, it was found that the thermodynamic character of the phase transition, whether it is first order or second order, is very sensitive to the cation order in the structure (Redfern and Salje 1987; Redfern et al. 1988). The cation order slightly influences the strains on the crystal structure, as shown above. Second, the spontaneous strains that accompany the phase transition are extremely sensitive to the cation order (Redfern and Salje 1987; Redfern et al. 1988). This somewhat surprising finding is consistent with the high degree of the sensitivity of the RUM spectrum to the imposed strains on the crystal described above.

It should be noted that in the idealized structure a soft mode occurs only at the relevant points Z and Z'. The frequency increases farther away from these points in all directions. This explains why Landau theory works so well for this phase transition. Fluctuations of the order parameter, which are neglected in Landau theory, are effectively confined to these wave vectors and are therefore never able to become thermodynamically significant.

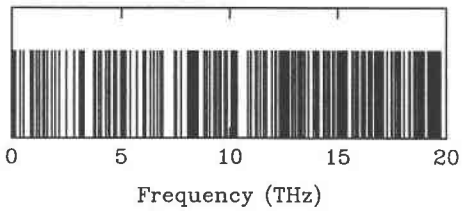

FIGURE 9. The distribution of frequencies in sanidine at $\mathbf{k} = 0$, where each mode is represented by a single vertical line. Note that there is a fairly uniform distribution of mode frequencies, with no clear gap between the RUMs, QRUMs, and the modes that are normally considered to be of higher frequency.

Quasi-RUMs in the feldspar structure

In feldspars there is a large set of QRUMs in addition to the RUMs with zero frequency. These occur for wave vectors all over the Brillouin zone. We illustrate the effect first by considering the frequencies given by our split-atom calculations using CRUSH. Figure 9 shows a line for each calculated frequency at $\mathbf{k} = 0$. It can be seen that there are no significant gaps between bands of modes, and instead the QRUM band merges continuously into the high-frequency band that is normally thought to contain the phonon modes that involve distortions of the tetrahedra. Figure 10 shows the frequency density of states calculated using CRUSH, integrated over the Brillouin zone. The picture of a broad spread of frequencies down to the lowest values is indicated by the observation that there is not the usual behavior $g(\omega) \propto \omega^2$ in the limit $\omega \rightarrow 0$ (see, for example, Dove 1993). To illustrate the spread of QRUMs in the Brillouin zone, the contour maps in Figure 11 show the magnitude of the sum $\Sigma\ 1/(\omega^2 + \Omega^2)$ for each wave vector, where Ω is a small constant as defined previously. At any wave vector a significant component of this sum comes from the QRUMs with large values of ω^{-2}, and variations across the Brillouin zone reflect the variations in the QRUM spectra. The three contour maps in Figure 11 show some a^*-b^* and b^*-c^* sections. The patterns of the contour plots are surprisingly complex.

The QRUMs help to explain the complex subsolidus behavior of feldspars. Because feldspar frameworks have QRUMs at wave vectors throughout the Brillouin zone, "local QRUMs" can form. Local QRUMs are superpositions of several low-frequency modes, this idea being similar to that of describing the motions of atoms in a crystal as a superposition of all possible normal modes. The local QRUMs are important because they can have a large amplitude in a small region of a crystal but a very low amplitude elsewhere. This implies that the feldspar framework can easily accommodate local defects because the framework can adjust about such a defect by means of the condensation of a local QRUM, the remainder of the framework remaining unaltered. Thus, Al-Si disorder and cation disorder do not strain the framework unduly, thereby allowing the large compositional range of feldspars observed in nature.

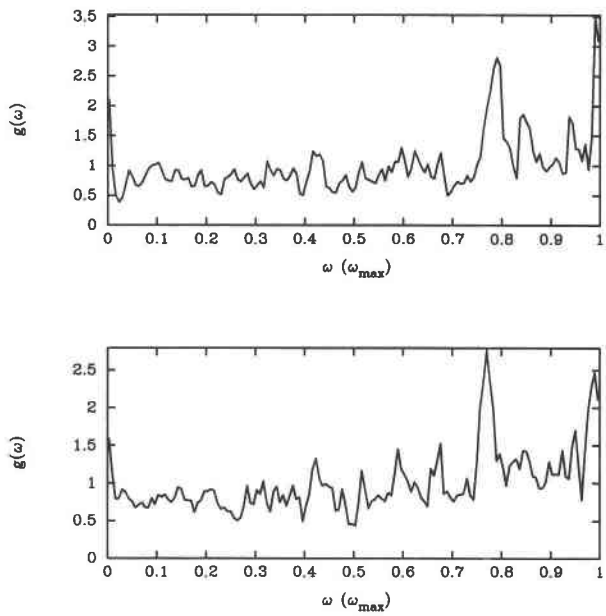

FIGURE 10. Phonon density of states for sanidine **(top)** and anorthite **(bottom)** evaluated using CRUSH.

SODALITE

The sodalite family of structures

Sodalites have the general formula $M_8T_{12}O_{24}X_2$, where M is a cage cation such as Na^+, Ca^{2+}, or Sr^{2+} (or a vacant site), T is a tetrahedrally coordinated framework cation such as Si^{4+} or Al^{3+} (it is common for these to be either all of one species or to have a 1:1 ratio of Si^{4+} to Al^{3+}), and X is a cage anion such as Cl^-, OH^-, SO_4^{2-}, or WO_4^{2-} (or another vacant site). Sodalites have a tetrahedral framework structure, the topology of which can be described in terms of a space-filling, body-centered packing of truncated octahedra. These truncated octahedra are commonly termed "sodalite cages." They are one of the fundamental building blocks of the more complex zeolite structures.

Sodalites can undergo various structural phase transitions (Depmeier 1992). The physical phenomena underlying these phase transitions may involve ordering of the tetrahedral cations, ordering of the cage cations or anions (the latter may also involve orientational ordering), or an adaptation (collapse) of the framework to the sizes of the cage ions in the way discussed above for kalsilite and nepheline. Changes in the sodalite structure as a function of composition are commonly explained by the adaptation of the sodalite framework to the size and geometry of the species incorporated into the cage. From this point of view, a sodalite would be fully expanded to the highest possible topological symmetry when large cage cations and anions are incorporated, or, in the case of large molecular cage anions such as SO_4^{2-} or WO_4^{2-}, where these are dynamically disordered. Incorporating smaller guest species into the host framework would then lead to a collapse of the framework with a significant volume re-

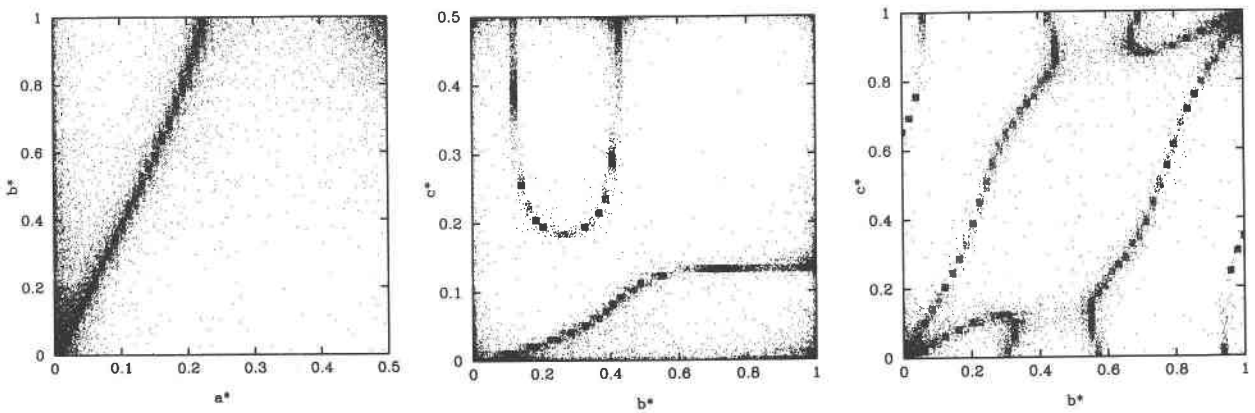

FIGURE 11. Contour maps of the function $\Sigma\ 1/(\omega^2 + \Omega^2)$ obtained from CRUSH calculations, evaluated by summing all modes for each wave vector, for all wave vectors in the a^*-b^* and b^*-c^* planes of sanidine (**left** and **center**) and the b^*-c^* plane of anorthite (**right**).

duction. For partially collapsed sodalites, the distortion from the fully expanded polymorph may be described in an ideal case by the tilt angle of the tetrahedra. This tilt angle is temperature and composition dependent, decreasing with increasing temperature and, as has been mentioned above, increasing for a given framework with decreasing radii of the cage ions.

The symmetries occurring in sodalites were recently reviewed by Depmeier (1992). The maximal symmetry of a fully expanded sodalite having only one species of tetrahedral cation, such as the aluminate sodalites, or having complete Al-Si disorder, is $Im\bar{3}m$. For the more common aluminosilicate sodalites, a sodalite with the same maximal topological symmetry would have a symmetry of $Pm3n$ because of the ordering of the two framework cations. An isotropic collapse of sodalites in these two space groups would lead to $I43m$ and $P43n$, respectively. The only known fully expanded sodalites are some aluminate sodalites, such as $Sr_8Al_{12}O_{24}(WO_4)_2$, with space group $Im\bar{3}m$, and ordered aluminosilicate sodalites, such as $Ag_6Si_6Al_6O_{24}$, with space group $Pm3n$.

Aside from the intrinsic interest in sodalite structures, sodalites are also interesting because the basic cage in the structure is incorporated into many zeolite structures, such as faujasite and zeolite A. Thus, the sodalite structure naturally leads into the field of zeolites, and results for sodalites may point toward important features of zeolites.

RUMs in the ideal $Im\bar{3}m$ structure

The RUM analysis for the ideal $Im\bar{3}m$ structure of sodalite is given in Table 3. The most striking result is that there is one RUM for each wave vector. This is a remarkable demonstration of the way in which symmetry can cause the constraints to become degenerate. In all our previous examples there were only lines or planes of RUMs in reciprocal space. Although these are significant, they represent only an infinitesimal fraction of reciprocal space, so that the total number of RUMs is on the order of zero in comparison with the total number of normal modes in a macroscopic crystal (i.e., for a line and a plane of RUMs, the ratio of the number of RUMs to the total number of modes is on the order of $N^{-1/3}$ and $N^{-2/3}$, respectively, where N is the number of unit cells). Sodalite is an example in which the number of RUMs is truly significant. With one RUM per wave vector, the structure is very floppy. Moreover, it is possible to generate local distortions of the structure as linear combinations of the RUMs over all wave vectors. Thus, a single cage can distort with only a low cost in energy and with no significant long-range effects. The implications for zeolite structures are clear: The RUM model provides a mechanism by which the structural cages can adapt their size and shape, thereby allowing for the characteristic catalytic properties of zeolites. This point is discussed in more detail below.

The important RUM in the ideal $Im\bar{3}m$ structure is the Γ_2^- mode. The condensation of this mode generates the more common $I\bar{4}3m$ phase, as found, for example, in $Ca_8Al_{12}O_{24}(WO_4)_2$. This is illustrated in Figure 12, which shows the structures of the $Im\bar{3}m$ and $I\bar{4}3m$ phases to illustrate the relationship between them through a RUM distortion. The RUMs at the N point have symmetry

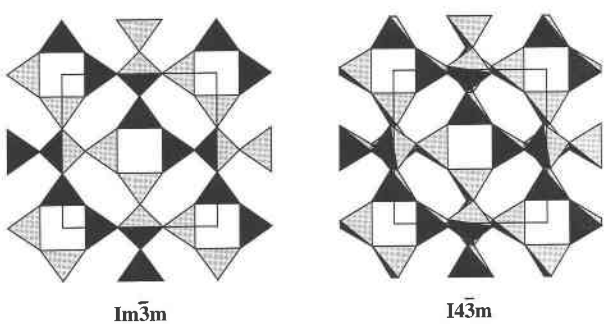

FIGURE 12. Framework structures of the two cubic sodalite phases with space groups $Im\bar{3}m$ and $I\bar{4}3m$, which is derived from the $Im\bar{3}m$ phase by condensation of the Γ_2^- RUM.

$2N_2^- + N_3^+$. The N_2^- RUMs can generate the $I4_1/acd$ structure formed as the low-temperature phases of $Sr_8Al_{12}O_{24}(MoO_4)_2$ and $Sr_8Al_{12}O_{24}(WO_4)_2$ (Depmeier and Bührer 1991).

RUMs in the $I\bar{4}3m$ and $P\bar{4}3n$ structures

The RUM calculations for the $I\bar{4}3m$ and $P\bar{4}3n$ phases are given in Table 3. There are several RUMs in these cases, although there is no longer one RUM per wave vector as in the ideal $Im\bar{3}m$ phase. It is quite likely that some of these act as soft modes for displacive phase transitions in representative examples, but the experimental situation as reflected in the literature seems to be lacking in crystallographic detail, and a detailed picture of phase transitions based on RUM distortions awaits further experimental data.

RUMs and the positioning of cations in sodalite structures

We return now to our discussion of the implications of having one RUM for each wave vector in the high-symmetry sodalite structure. As in the case of nepheline, static RUM displacements can cause O atoms to move inward toward some site, and this is a self-regulating mechanism for holding cations in place. In the case of sodalite the Γ_2^- RUM involves cooperative rotations of the tetrahedra about their local $\bar{4}$ axes, the effect of which on the hexagonal rings is to bring three of the O atoms inward toward the center and three outward. To be precise, they move toward a position a little above or below the plane of the ring. This is the position where most cation species are found in zeolites with the sodalite cage structure (Mortier 1982).

In sodalite, the existence of one RUM per wave vector is the basis of an important new phenomenon, namely the existence of local RUMs formed as linear combinations of RUMs in reciprocal space. These lead to local adsorption sites, formed as local wave packets, which need not be repeated periodically in each unit cell. The wider the region of reciprocal space used in these wave packets, the more localized the wave packet can be. By using the band of RUMs over the whole of the Brillouin zone, we can construct a local RUM distortion that is localized on one six-membered ring and its six nearest-neighbor rings (Hammonds et al., in preparation).

This phenomenon has application to other zeolites with the cage structure of sodalite, such as LTA and faujasite. These zeolites are known to bind cations locally at various sites, including those described above for sodalite (George et al. 1991). In zeolite LTA there are seven complete bands of RUMs, from which a variety of localized RUMs can be formed, which may explain some of the binding sites in this material (Dove et al. 1996a).

Leucite

Phase transitions in the leucite structures

Above 960 K, leucite, $KAlSi_2O_6$, has a cubic structure with space group $Ia3d$, but on cooling it undergoes two successive displacive phase transitions (Palmer et al. 1989, 1990, 1997; Palmer and Salje 1990). The first transition is to a tetragonal structure with space group $I4_1/acd$. The second transition at 940 K is to another tetragonal structure with space group $I4_1/a$. The transitions are rapid, reversible, and continuous (second order), and they do not appear to involve any Al-Si ordering (Dove et al. 1992). The cubic phase is necessarily disordered with respect to the site ordering of the Al and Si atoms. By replacing the K cation with Rb or Cs the transition temperatures are lowered, but the same $I4_1/a$ phase exists in these isomorphs at low temperatures (Palmer et al. 1997). The transitions generate considerable strain, and indeed the $Ia3d$-$I4_1/acd$ transition has the symmetry change consistent with a proper ferroelastic phase transition (Cowley 1976; Stokes and Hatch 1988).

It is possible to replace the framework cations with other atoms and to retain the basic leucite structure. For example, $KFeSi_2O_6$ undergoes a first-order transition between the $Ia3d$ and $I4_1/a$ phases at 930 K (Palmer et al. 1997). The Mg-substituted leucite $K_2MgSi_5O_{12}$ can exist in two distinct states (Bell et al. 1984, 1993). The cubic $Ia3d$ phase has the Mg and Si cations disordered. However, it is easy to produce a form of Mg-substituted leucite with complete order, and the structure in this case is monoclinic with space group $P2_1/c$. On heating this phase transforms to an orthorhombic phase with space group $Pbca$ by a displacive mechanism (Redfern 1994). There is considerable interest in the different structures that are found in the leucite family because the correlation between structure and chemistry may provide some useful insights into the structural chemistry of other silicates.

RUMs in the $Ia3d$ structure

The RUM analysis of the $Ia3d$ phase is given in Table 3. In comparison with some of the other examples in this paper there are not many RUMs in this phase, and those that do exist are all restricted to a single symmetry direction in reciprocal space, namely along ⟨110⟩. The existence of this line of RUMs was confirmed by the inelastic neutron-scattering study of $KAlSi_2O_6$ leucite reported by Boysen (1990), as discussed by Dove et al. (1995).

RUMs in the $I4_1/acd$ and $I4_1/a$ structures

The RUM analysis for the $I4_1/acd$ leucite structure is given in Table 4. There are no RUMs in the $I4_1/a$ leucite structure, and the number of RUMs in the $I4_1/acd$ structure is slightly less than in the parent $Ia3d$ structure.

The phase transitions in leucite

The symmetry analysis of the displacive phase transitions in $KAlSi_2O_6$ depends on the exact sequence of transitions. The two transition sequences, $Ia3d$-$I4_1/a$ directly and $Ia3d$-$I4_1/acd$-$I4_1/a$ as observed, each involve distortions at zero wave vector. If the phase transition were to be directly from $Ia3d$ to $I4_1/a$ the transition would be generated by a distortion of T_{1g} symmetry. On the other hand, for the transition to proceed through the interme-

diate $I4_1/acd$ phase, the initial distortion of the cubic phase has symmetry E_g, and the subsequent distortion of the $I4_1/acd$ phase to generate the $I4_1/a$ structure has symmetry A_{2g} in the point group $4/mmm$. The transition $Ia3d$-$I4_1/acd$ has the correct symmetry change to be a proper ferroelastic phase transition with a soft acoustic mode rather than a soft optic mode.

The optic RUMs with zero wave vector in the $Ia3d$ structure have symmetry $A_{2g} + A_{2u} + T_{1g}$. None of the RUMs has E_g symmetry, which means that the transition $Ia3d$-$I4_1/acd$ does not involve a soft optic RUM. There is, however, a soft transverse acoustic RUM at zero wave vector. The three acoustic modes at $\mathbf{k} = 0$ have symmetry T_{1u}, with the transverse components generating shear strains of symmetry E_g. Thus, the first stage of the transition, namely $Ia3d$-$I4_1/acd$, is a proper ferroelastic instability. The RUMs with zero wave vector in the $I4_1/acd$ phase have symmetries $A_{2g} + B_{1g} + B_{1u}$ (the RUMs in the cubic phase transformed as $A_{2g} \rightarrow B_{1g}$, $A_{2u} \rightarrow B_{1u}$, and $T_{1g} \rightarrow A_{2g} + E_g$, although the latter E_g is not a RUM in the $I4_1/acd$ phase). The A_{2g} RUM then acts as the soft mode to drive the transition $I4_1/acd$-$I4_1/a$. This picture was corroborated to some extent by the inelastic neutron-scattering measurements of Boysen (1990), which showed the existence of the soft optic and acoustic RUMs. Now that the RUM model has been used to give the overall picture it would be worth extending the experimental data.

The effect of chemical doping

It is interesting to consider further the substitution of the K^+ cations in the leucite structure by Rb^+ and Cs^+. The effect, as noted above, is to lower the transition temperature on substitution (Palmer et al. 1997). Moreover, the maximum distortion, that at 0 K, decreases on substitution of larger cations. The experimental data are given in Table 6. On the basis of general considerations of the RUM model (Dove et al. 1992) we predict that the transition temperature T_c varies as the square of the order parameter Q. For the $Ia3d$-to-$I4_1/a$ phase transition in leucite we expect that the volume change ΔV also varies as Q^2, so that we expect $T_c \propto \Delta V$. The data given in Table 6 show that this relationship is followed to a reasonable level. However, we must not push the quantitative analysis too far, for the behavior of each of the different substituted leucite samples is not identical.

Another interesting observation is that the unit-cell parameter of the cubic phase of leucite also increases on substitution of the larger cations. Table 6 gives the cubic unit-cell parameters of the three leucite samples given above, together with the unit-cell parameter for analcime, $NaAlSi_2O_6 \cdot H_2O$ (Line et al. 1996), and dehydrated analcime, $NaAlSi_2O_6$ (Line et al., in preparation), with the unit-cell parameters in each case either measured at 1000 K or extrapolated to 1000 K from data at lower temperatures. The data imply that the Si-O and Al-O bond lengths apparently depend on the substitution of the K^+ cation. This is rather surprising because the substitution cannot affect the sizes of the tetrahedra, and from our calculations with the IDEALISER program we found that the unit-cell parameter of leucite is uniquely determined by the tetrahedral bond lengths without any possibility for rotations of the tetrahedra to change the unit-cell volume without a change in symmetry. Instead the RUM model suggests an alternative explanation in which the change in bond length is probably associated with apparent shortening resulting from thermal librational motions of the tetrahedra moving as rigid bodies (as discussed by Downs et al. 1990, 1992). This occurs because the cubic phase has the maximum possible volume for this structure topology, without any collapse of the framework about the cage cations. The effect of any RUM distortion, dynamic or static, is to reduce the volume of the structure. This is illustrated in Figure 1, where the reduction in the unit-cell parameter is proportional to θ^2, the square of the rotation angle of the rigid units. Similarly, any RUM phonon mode causes a decrease in the volume of the cubic phase by an amount proportional to $\langle\theta^2\rangle$, where the angle brackets denote an average value because of thermal libration, particularly from the RUMs with low frequency and hence large amplitude. Two consequences follow from this picture. First, the apparently shorter bond lengths are associated with larger amplitude motions. If there is a cation or H_2O molecule in the cavities, this object hinders the librational motion, just as it hinders the structural collapse associated with the phase transition. Thus, we expect the amplitudes for rigid tetrahedral rotations to be largest for natural leucite (with K cations) and smallest for Cs-exchanged leucite and analcime, leading to a smaller cell parameter in natural leucite (which is about the same size as in dehydrated analcime) and larger cell parameters in Cs-exchanged leucite and analcime. This is confirmed by the data in Table 6. Second, it might be anticipated that $\langle\theta^2\rangle$ scales with temperature, so that at higher temperatures the mean-square amplitude is larger, leading to a greater reduction in the volume and hence a negative thermal expansion. In fact, the thermal expansion in the leucite samples and in analcime is positive (Palmer et al. 1997; Line et al. 1996), but it is negative in dehydrated analcime (Line et al., in preparation).

TABLE 6. Lattice parameters for cubic leucite structures, measured at or extrapolated to 1000 K, transition temperatures and relative volume changes for different leucite samples

Leucite sample	a (Å)	T_c (K)*	ΔV (Å^3)*
$KAlSi_2O_6$	13.55*	936	99
$RbAlSi_2O_6$	13.62*	750	65
$CsAlSi_2O_6$	13.73*	373	38
$NaAlSi_2O_6 \cdot H_2O$ (analcime)	13.80**		
$NaAlSi_2O_6$ (dehydrated analcime)	13.56**		

Note: The relative volume changes are those measured at ⅔ of the transition temperature.
* Data from Palmer et al. (1996).
** Data from Line et al. (1996).

RUMs in the *Pbca* structure

The RUM analysis for the *Pbca* leucite indicated no optic RUMs but found that along the three principal axes there is a single transverse acoustic RUM with frequency that varies as $\omega \propto k^2$. The softest acoustic mode is with the wave vector along [101] and polarized along [110]. Thus, we predict that the phase transition in Mg-substituted leucite from *Pbca* to $P2_1/c$ is a proper ferroelastic phase transition driven by a soft acoustic mode. This is consistent with the symmetry tables of Stokes and Hatch (1988).

Cordierite

RUMs in the cordierite structures

Cordierite, $Mg_2Al_4Si_5O_{18}$, initially crystallizes in a hexagonal structure, space group *P6/mcc*, which is disordered with regard to the Al-Si site occupancies (Meagher and Gibbs 1977). On annealing at high temperatures it transforms into an ordered orthorhombic phase with space group *Cccm* (Gibbs 1966; Putnis et al. 1987). Cordierite has attracted considerable technological interest, partly because of the negative linear thermal expansion coefficient in one direction and the subsequent near-zero value of the volume thermal expansion coefficient (Smart and Glasser 1977).

The RUM data for the hexagonal and orthorhombic phases of cordierite are given in Tables 1 and 4, respectively. These two structures contain a reasonable number of RUMs.

Anomalous thermal expansion of cordierite

In our discussion of the volumes of the different cubic leucite structures, we explained the volume differences as the effects of thermal vibrations involving rigid-body rotations of the tetrahedra. It was noted that these vibrations lower the volume of the structure. They are also of relatively large amplitude because the square of the amplitude scales as ω^{-2} (Dove 1993), where the angular frequency ω of the RUM is quite low. In the case of the leucite structures we interpreted the difference in volume as resulting from the cage cations acting to inhibit the amplitude. In other cases, such as cordierite, dehydrated analcime, and β-quartz, the thermal vibrations decrease volume on heating. The square of the amplitude scales as k_BT/ω^2 (Dove 1993), so that there is a contribution to the volume $\propto -k_BT/\omega^2$. This negative contribution to the thermal expansion is the opposite of that from the anharmonic expansion of the Si-O bonds. In the case of cordierite this negative contribution partly results from several RUMs. Although we have not attempted to quantify this point, we believe that the RUM model leads to a general understanding of the phenomenon of negative or anomalously low thermal expansion in some silicates.

Discussion and summary

Our purpose in the present paper has been to explore the generality of the RUM model by calculating the RUM spectra for a range of framework aluminosilicates and relating the results of these calculations to some of the properties of these materials. The major focus has been the displacive phase transitions that are so common in framework aluminosilicates. Indeed, the existence of RUMs naturally explains why phase transitions may occur in these materials. We noted that the RUMs can act as the classical soft modes for these phase transitions, and we identified both optic RUMs and acoustic RUMs that can act as the soft mode in the various examples.

In view of one of the arguments presented in the second section, it might seem surprising that there are any RUMs at all. Instead, there are RUMs in all the systems we studied, but for any given structure the number of RUMs decreases as the symmetry is lowered as a result of displacive phase transitions. Because several RUMs act as candidate soft modes, several potential instabilities may be possible for any framework aluminosilicate. The question of why any given structure should choose to distort by one RUM as opposed to any other is outside the scope of the present paper, but we showed that the torsional interaction that preserves the Si-O-Si bond angles can separate the energies of different RUM distortions. Further discussion of this point in general terms is given elsewhere (Dove et al. 1995).

In some cases the high-temperature phases are expected to be disordered. Cristobalite and tridymite are obvious examples of this because the ideal structures imply the existence of implausible linear Si-O-Si bonds. The nature of the high-temperature phases is an open question, but we argued that the superposition of planes of RUMs can produce dynamic disorder on the length scale of the unit cell. We prefer this description rather than the idea that a high-temperature phase is composed of domains having the local structure of the low-temperature phase, as was outlined in our discussion of cristobalite.

Some of our calculations have received experimental confirmation. Inelastic neutron-scattering experiments have measured several low-frequency modes in quartz (Dolino et al. 1992) and leucite (Boysen 1990) that are calculated to be RUMs. In quartz one of the modes that is a RUM only in the high-temperature phase is seen to increase rapidly in frequency on cooling below the transition temperature. The RUMs in cristobalite (Hua et al. 1988; Welberry et al. 1989) and tridymite (Withers et al. 1994) have been measured by electron diffraction, providing a stringent test of the calculated RUM spectra in the different phases of these materials. One striking feature of these observations is that the streaks of diffuse scattering that correspond to the scattering plane cutting through planes of RUMs in reciprocal space are narrow (apparently no wider than the resolution of the experiment). Inelastic neutron-scattering measurements on a powdered sample of cristobalite (Swainson and Dove 1993a) have shown that there is a striking difference in the number of low-frequency modes (i.e., RUMs) between the high-temperature and low-temperature phases, in agreement with the calculated RUM spectra. Thus,

there is already a strong body of experimental evidence in support of the RUM model.

We noted some of the consequences of the existence of RUMs aside from the main focus on the origins of displacive phase transitions. One is that RUM distortions are involved in cation-ordering processes. When Na and K order in the kalsilite-nepheline solid-solution series, the structure of the ideal parent phase must distort to accommodate the different sizes of the Na^+ and K^+ cations. We have seen how these structures distort to accommodate the different cation sizes by RUM distortions.

Another consequence of the existence of RUMs is that a RUM vibration is expected to lower the volume of a structure. In the case of the leucite-analcime family of structures, the presence of a cation or H_2O molecule in the cages in the structure can inhibit the amplitude of the RUM vibrations, which leads to a change in the volume of the structure for different substitutions. Because the RUM vibrational amplitude increases with temperature, the RUMs provide a negative contribution to the thermal expansion. This has been documented for cristobalite (Swainson and Dove 1995b), and we speculate that the model can provide the basis for understanding the observation of negative thermal expansion in β-quartz, cordierite, dehydrated analcime, and some zeolites.

We have not attempted in this paper to cover systematically all framework topologies, but hope that the present study, together with the availability of our CRUSH program (Hammonds et al. 1994), will encourage analysis of other systems. We have also limited the amount of information given for each system; for example, we have not given detailed information on the eigenvectors of each RUM, nor have we given the symmetries of the RUMs unless they were relevant for the discussion of a phase transition. However, this information can easily be generated by the interested reader using the CRUSH program.

Finally, we pose the question of where the insights from the RUM model will subsequently lead. The two major areas in which the RUM model may have some impact are studies of silicate glasses and zeolites. It is worth recalling that the basic idea of RUMs as floppy modes is already common in the study of glasses. However, in the case of glasses no systematic account has been made of the way in which constraints can be degenerate, although the existence of local RUMs has been observed by low-frequency inelastic neutron scattering. We imagine that RUMs exist in glasses because of the existence of large rings of connected tetrahedra, which seem to allow for greater degeneracies of constraints. The step from the evaluation of RUMs in crystalline networks to the analysis of RUMs in glassy networks is not trivial, but we believe that there are enough pointers in our present work to make it quite feasible. We expect that a more systematic analysis of the RUMs in glassy networks will allow some of the fundamental and technologically important physical properties, such as thermal expansion, to be better understood, particularly with regards to the dependence on chemical composition. The application of the RUM model to zeolites will be somewhat easier, and as we noted in the discussion on sodalites some preliminary calculations have already been made. Given that in some cases there is one or more RUMs per wave vector, there is the possibility of considerable local distortion of the zeolite cages without significant cost to the energy of the structure. It is quite likely that this would be related to the catalytic properties of zeolites. Moreover, the large number of RUMs would also explain the frequent observations of negative thermal expansion in zeolites. We envisage that a RUM analysis will thus form part of the routine evaluation of any custom-designed zeolite structure.

Acknowledgments

We are pleased to acknowledge helpful discussions with our Cambridge colleagues Ian Swainson (now at Chalk River, Canada), Peter Sollich (now in Edinburgh), Michael Carpenter, Andrew Putnis, Simon Redfern, Ekhard Salje, Bernd Wruck, David Palmer, and Richard de Dombal. We are particularly indebted to Marcel Vallade (Grenoble) for sharing his ideas with us in detail long before publication. As noted in our discussion of quartz, he was the first person to consider and calculate all the RUMs that a given structure allows, and it was this that inspired the present work. We thank Larry Finger (Washington) for providing us with preliminary details of the crystal structure of the high-pressure phase of cristobalite prior to publication. We also thank David Palmer for the use of his CrystalMaker program in the preparation of some of our figures. Finally, we are grateful to the NERC, SERC-EPSRC, and the Royal Society (U.K.) for financial support.

References cited

Andou, Y., and Kawahara, A. (1984) The refinement of the structure of synthetic kalsilite. Mineralogical Journal, 12, 153–161.

Bell, A.M.T., Henderson, C.M.B., Redfern, S.A.T., Cernik, R.J., Champness, P.E., Fitch, A.N., and Kohn, S.C. (1984) Structures of synthetic $K_2MgSi_5O_{12}$ leucites by integrated X-ray powder diffraction, electron diffraction and ^{29}Si MAS NMR methods. Acta Crystallographica, B50, 31–41.

Bell, A.M.T., Cernik, R.J., Champness, P.E., Fitch, A.N., Henderson, C.M.B., Kohn, S.C., Norledge, B.V., and Redfern, S.A.T. (1993) Crystal structures of leucites from synchrotron X-ray powder diffraction data. Materials Science Forum, 133–136, 697–702.

Berge, B., Bachheimer, J.P., Dolino, G., Vallade, M., and Zeyen, C.M.E. (1986) Inelastic neutron scattering study of quartz near the incommensurate phase transition. Ferroelectrics, 66, 73–84.

Bethke, J., Dolino, G., Eckold, G., Berge, B., Vallade, M., Zeyen, C.M.E., Hahn, T., Arnold, H., and Moussa, F. (1987) Phonon dispersion and mode coupling in high-quartz near the incommensurate phase transition. Europhysics Letters, 3, 207–212.

Boisen, M.B., Jr., Gibbs, G.V., Downs, R.T., and D'Arco, P. (1990) The dependence of the SiO bond length on structural parameters in coesite, the silica polymorphs, and the clathrasils. American Mineralogist, 75, 748–754.

Boysen, H. (1990) Neutron scattering and phase transitions in leucite. In E.K. Salje, Ed., Phase transitions in ferroelastic and co-elastic crystals, p. 334–349. Cambridge University Press, Cambridge, U.K.

Boysen, H., Dorner, B., Frey, F., and Grimm, H. (1980) Dynamic structure determination for two interacting modes at the M-point in α- and β-quartz by inelastic neutron scattering. Journal of Physics C: Solid State Physics, 13, 6127–6146.

Buchenau, U., Nucker, N., and Dianoux, A.J. (1984) Neutron scattering study of the low-frequency vibrations in vitreous silica. Physical Review Letters, 53, 2316–2319.

Buchenau, U., Prager, M., Nucker, N., Dianoux, A.J., Ahmad, N., and

Phillips, W.A. (1986) Low-frequency modes in vitreous silica. Physical Review B, 34, 5665–5673.

Cai, Y., and Thorpe, M.F. (1989) Floppy modes in network glasses. Physical Review B, 40, 10535–10542.

Capobianco, C., and Carpenter, M. (1989) Thermally induced changes in kalsilite ($KAlSiO_4$). American Mineralogist, 74, 797–811.

Carpenter, M.A. (1988) Thermochemistry of aluminium/silicon ordering in feldspar minerals. In E. Salje, Ed., Physical properties and thermodynamic behavior of minerals, p. 265–323. Reidel, Dordrecht, the Netherlands.

Cowley, R.A. (1976) Acoustic phonon instabilities and structural phase transitions. Physical Review B, 13, 4877–4885.

Depmeier, W. (1992) Remarks on symmetries occurring in the sodalite family. Zeitschrift für Kristallographie, 199, 75–89.

Depmeier, W., and Bührer, W. (1991) Aluminate sodalites: $Sr_8[Al_{12}O_{24}](MoO_4)_2$ (SAM) at 293, 423, 523, 623 and 723 K and $Sr_8[Al_{12}O_{24}](CrO_4)_2$ (SAW) at 293 K. Acta Crystallographica, B47, 197–206.

Döhler, G.H., Dandoliff, R., and Bilz, H. (1980) A topological-dynamical model of amorphicity. Journal of Non–Crystalline Solids, 42, 87–96.

Dolino, G. (1990) The α-inc-β transitions of quartz: A century of research on displacive phase transitions. Phase Transitions, 21, 59–72.

Dolino, G., Berge, B., Vallade, M., and Moussa, F. (1989) Inelastic neutron scattering study of the origin of the incommensurate phase of quartz. Physica, B156, 15–16.

——— (1992) Origin of the incommensurate phase of quartz: I. Inelastic neutron scattering study of the high temperature β phase of quartz. Journal de Physique, I-2, 1461–1480.

Dollase, W.A. (1967) The crystal structure at 220 °C of orthorhombic high tridymite from the Steinbach meteorite. Acta Crystallographica, 23, 617–623.

Dolling, G., Powell, B.M., and Sears, V.F. (1979) Neutron diffraction study of the plastic phases of polycrystalline SF_6 and CBr_4. Molecular Physics, 37, 1859–1883.

Dove, M.T. (1989) On the computer modeling of diopside: Toward a transferable potential for silicate minerals. American mineralogist, 74, 774–779.

——— (1993) Introduction to lattice dynamics, 258 p. Cambridge University Press, Cambridge, U.K.

——— (1997) Theory of displacive phase transitions in minerals. American Mineralogist, 82, in press.

Dove, M.T., Pawley, G.S., Dolling, G., and Powell, B.M. (1986) Collective excitations in an orientationally frustrated solid: Neutron scattering and computer simulation studies of SF_6. Molecular Physics, 57, 865–880.

Dove, M.T., Giddy, A.P., and Heine, V. (1991) Rigid unit mode model of displacive phase transitions in framework silicates. Transactions of the American Crystallographic Association, 27, 65–74.

——— (1992) On the application of mean-field and Landau theory to displacive phase transitions. Ferroelectrics, 136, 33–49.

Dove, M.T., Cool, T., Palmer, D.C., Putnis, A., Salje, E.K.H., and Winkler, B. (1993) On the role of Al-Si ordering in the cubic-tetragonal phase transition in leucite. American Mineralogist, 78, 486–492.

Dove, M.T., Heine, V., and Hammonds, K.D. (1995) Rigid unit modes in framework silicates. Mineralogical Magazine, 59, 629–639.

Dove, M.T., Gambhir, M., Hammonds, K.D., Heine, V., and Pryde, A.K.A. (1996a) Distortions of framework structures. Phase Transitions, in press.

Dove, M.T., Hammonds, K.D., Heine, V., Withers, R.L., Xiao, Y., and Kirkpatrick, R.J. (1996b) Rigid unit modes in the high-temperature phase of SiO_2 tridymite: Calculations and electron diffraction. Physics and Chemistry of Minerals, 23, 55–61.

Dove, M.T., and Redfern, S.A.T. (1997) Lattice simulation studies of the ferroelastic phase transitions in $(Na,K)AlSi_3O_8$ and $(Sr,Ca)Al_2Si_2O_8$ feldspar solid solutions. American Mineralogist, 82, in press.

Downs, R.T., Gibbs, G.V., and Boisen, M.B., Jr. (1990) A study of the mean-square displacement amplitudes of Si, Al, and O atoms in framework structures: Evidence for rigid bonds, order, twinning, and stacking-faults. American Mineralogist, 75, 1253–1267.

Downs, R.T., Gibbs, G.V., Bartelmehs, K.L., and Boisen, M.B., Jr. (1992) Variations of bond lengths and volumes of silicate tetrahedra with temperature. American Mineralogist, 77, 751–757.

George, A.R., Catlow, C.R.A., and Thomas, J.M. (1991) Determining the environment of transition metal ions in zeolitic catalysts: A combined computational and synchrotron-based study of nickel ions in zeolite-Y. Catalysis Letters, 8, 193–200.

Gibbs, G.V. (1966) The polymorphism of cordierite: I. The crystal structure of low cordierite. American Mineralogist, 51, 1068–1087.

Gibbs, G.V., Downs, J.W., and Boisen, M.B., Jr. (1994) The elusive Si-O bond. In Mineralogical Society of America Reviews in Mineralogy, 29, 331–368.

Giddy, A.P., Dove, M.T., Pawley, G.S., and Heine, V. (1993) The determination of rigid unit modes as potential soft modes for displacive phase transitions in framework crystal structures. Acta Crystallographica, A49, 697–703.

Grimm, H., and Dorner, B. (1975) On the mechanism of the α-β phase transformation of quartz. Physics and Chemistry of Solids, 36, 407–413.

Hammonds, K.D., Dove, M.T., Giddy, A.P., and Heine, V. (1994) Crush: A Fortran program for the analysis of the rigid-unit mode spectrum of a framework structure. American Mineralogist, 79, 1207–1209.

Hatch, D.M., and Ghose, S. (1991) The α-β phase transition in cristobalite, SiO_2. Physics and Chemistry of Minerals, 17, 554–562.

Hazen, R.M., and Finger, L.W. (1982) Comparative crystal chemistry: Temperature, pressure, composition and the variation of crystal structure. Wiley, Chichester, U.K.

He, H., and Thorpe, M.F. (1985) Elastic properties of glasses. Physical Review Letters, 54, 2107–2110.

Hua, G.L., Welberry, T.R., Withers, R.L., and Thompson, J.G. (1988) An electron diffraction and lattice-dynamical study of the diffuse scattering in β-cristobalite, SiO_2. Journal of Applied Crystallography, 21, 458–465.

Kihara, K. (1978) Thermal change in unit-cell dimensions, and a hexagonal structure of tridymite. Zeitschrift für Kristallographica, 148, 237–253.

Lasaga, A.C., and Gibbs, G.V. (1987) Applications of quantum mechanical potential surfaces to mineral physics calculations. Physics and Chemistry of Minerals, 14, 107–117.

——— (1988) Quantum mechanical potential surfaces and calculations of minerals and molecular clusters. Physics and Chemistry of Minerals, 16, 29–41.

Line, C.M.B., Dove, M.T., Knight, K.S., and Winkler, B. (1996) The low-temperature behaviour of analcime: I. High-resolution neutron powder diffraction. Mineralogical Magazine, 60, 499–507.

Marians, C.S., and Burdett, J.K. (1990) Geometric constraints: A refined model for the structure of silica glass. Journal of Non-Crystalline Solids, 124, 1–21.

Marians, C.S., and Hobbs, L.W. (1990a) Local structure of silica glasses. Journal of Non-Crystalline Solids, 119, 269–282.

——— (1990b) Network properties of crystalline polymorphs of silica. Journal of Non-Crystalline Solids, 124, 242–253.

McGuinn, M.D., and Redfern, S.A.T. (1994a) Ferroelastic phase transition in $SrAl_2Si_2O_8$ feldspar at elevated pressure. Mineralogical Magazine, 58, 21–26.

——— (1994b) Ferroelastic phase transition along the join $CaAl_2Si_2O_8$-$SrAl_2Si_2O_8$. American Mineralogist, 79, 24–30.

Meahger, E.P., and Gibbs, G.V. (1977) The polymorphism of cordierite: II. The crystal structure of indialite. Canadian Mineralogist, 15, 43–49.

Megaw, H.D. (1973) Crystal structures: A working approach, 563 p. Saunders, Philadelphia, Pennsylvania.

Merlino, S. (1984) Feldspathoids: The average and real structures. In W.L. Brown, Ed., Feldspars and feldspathoids, p. 435–470. Reidel, Dordrecht, the Netherlands.

Mortier, W.J. (1982) Extra framework sites in zeolites, 67 p. Butterworth, London, U.K.

Palmer, D.C., Salje, E.K.H., and Schmahl, W.W. (1989) Phase transitions in leucite: X-ray diffraction studies. Physics and Chemistry of Minerals, 16, 714–719.

Palmer, D.C., Bismayer, U., and Salje, E.K.H. (1990) Phase transitions in leucite: Order parameter behavior and the landau potential deduced from Raman-spectroscopy and birefringence studies. Physics and Chemistry of Minerals, 17, 259–265.

Palmer, D.C., and Salje, E.K.H. (1990) Phase transitions in leucite: Di-

electric properties and transition mechanism. Physics and Chemistry of Minerals, 17, 444–452.

Palmer, D.C., and Finger, L.W. (1994) Pressure-induced phase transition in cristobalite: An X-ray powder diffraction study to 4.4 GPa. American Mineralogist, 79, 1–8.

Palmer, D.C., Dove, M.T., Ibberson, R.M., and Powell, B.M. (1997) Structural behavior, crystal chemistry and phase transitions in substituted leucites: High-resolution neutron powder diffraction. American Mineralogist, 82, in press.

Patel, A., Price, G.D., and Mendelssohn, M.J. (1991) A computer simulation approach to modelling the structure, thermodynamic and oxygen isotope equilibria of silicates. Physics and Chemistry of Minerals, 17, 690–699.

Pawley, G.S. (1972) Analytic formulation of molecular lattice dynamics based on pair potentials. Physica Status Solidi, 49b, 475–488.

Phillips, B.L., Thompson, J.G., Xiao, Y., and Kirkpatrick, R.J. (1993) Constraints on the structure and dynamics of the β-cristobalite polymorphs of SiO_2 and $AlPO_4$ from ^{31}P, ^{27}Al and ^{29}Si NMR spectroscopy from 770 K. Physics and Chemistry of Minerals, 20, 341–352.

Putnis, A. (1992) Introduction to mineral sciences, 457 p. Cambridge University Press, Cambridge, U.K.

Putnis, A., Salje, E., Redfern, S.A.T., Fyfe, C.A., and Stobl, H. (1987) Structural states of Mg-cordierite: I. Order parameters from synchrotron X-ray and NMR data. Physics and Chemistry of Minerals, 14, 446–454.

Redfern, S.A.T. (1994) Cation ordering patterns in leucite-related compounds. In A. Putnis, Ed., Proceedings of the workshop on kinetics of cation ordering, European Science Foundation Programme on kinetic processes in minerals and ceramics. European Science Foundation, Cambridge, U.K.

Redfern, S.A.T., and Salje, E.K.H. (1987) Thermodynamics of plagioclase: II. Temperature evolution of the spontaneous strain at the $I\bar{1}$-$P\bar{1}$ phase transition in anorthite. Physics and Chemistry of Minerals, 14, 189–195.

Redfern, S.A.T., Graeme-Barber, A., and Salje, E.K.H. (1988) Thermodynamics of plagioclase: III. Spontaneous strain at the $I\bar{1}$-$P\bar{1}$ phase transition in Ca-rich plagioclase. Physics and Chemistry of Minerals, 16, 157–163.

Redfern, S.A.T., and Salje, S.A.T. (1992) Microscopic dynamic and macroscopic thermodynamic character of the $I\bar{1}$-$P\bar{1}$ phase transition in anorthite. Physics and Chemistry of Minerals, 18, 526–533.

Salje, E. (1985) Thermodynamics of sodium feldspar: I. Order parameter treatment and strain induced coupling effects. Physics and Chemistry of Minerals, 12, 93–98.

——— (1987) Thermodynamics of plagioclases I: Theory of the $I\bar{1}$-$P\bar{1}$ phase transition in anorthite and Ca-rich plagioclases. Physics and Chemistry of Minerals, 14, 181–188.

——— (1990) Phase transitions in ferroelastic and co-elastic crystals, 366 p. Cambridge University Press, Cambridge, U.K.

Sapriel, J. (1975) Domain wall orientations in ferroelastics. Physical Review B, 12, 5128.

Schmahl, W.W., Swainson, I.P., Dove, M.T., and Graeme-Barber, A. (1992) Landau free energy and order parameter behaviour of the α-β phase transition in cristobalite. Zeitschrift für Kristallographie, 201, 125–145.

Smart, R.M., and Glasser, F.P. (1977) Stable cordierite solid solutions in the MgO-Al_2O_3-SiO_2 system: Composition, polymorphism and thermal expansion. Science of Ceramics, 9, 256–263.

Sollich, P., Heine, V., and Dove, M.T. (1994) The Ginzburg interval in soft mode phase transitions: Consequences of the rigid unit mode picture. Journal of Physics: Condensed Matter, 6, 3171–3196.

Spearing, D.R., Farnan, I., and Stebbins, J.F. (1992) Dynamics of the α-β phase transitions in quartz and cristobalite as observed by in situ high-temperature ^{29}Si and ^{17}O NMR. Physics and Chemistry of Minerals, 19, 309–321.

Stirling, W.G. (1972) Neutron inelastic scattering study of the lattice dynamics of strontium titanate: Harmonic models. Journal of Physics C: Solid State Physics, 5, 2711–2730.

Stokes, H.T., and Hatch, D.M. (1988) Isotropy subgroups of the 230 crystallographic space groups. World Scientific, Singapore.

Swainson, I.P., and Dove, M.T. (1993a) Low-frequency floppy modes in β-cristobalite. Physical Review Letters, 71, 193–196.

——— (1993b) Comment on "First-principles studies on structural properties of β-cristobalite." Physical Review Letters, 71, 3610.

——— (1995a) Molecular dynamics simulation of α- and β-cristobalite. Journal of Physics: Condensed Matter, 7, 1771–1788.

——— (1995b) On the thermal expansion of β-cristobalite. Physics and Chemistry of Minerals, 22, 61–65.

Swainson, I.P., Dove, M.T., Palmer, D.C., and Poon, W.C-K. (1996) Infrared and Raman spectroscopic studies of the α-β phase transition in cristobalite. Physics and Chemistry of Minerals, submitted.

Tautz, F.S., Heine, V., Dove, M.T., and Chen, X. (1991) Rigid unit modes in the molecular dynamics simulation of quartz and the incommensurate phase transition. Physics and Chemistry of Minerals, 18, 326–336.

Thorpe, M.F. (1983) Continuous deformations in random networks. Journal of Non-Crystalline Solids, 57, 355–370.

Tribaudino, M., Benna, P., and Bruno, E. (1993) $I\bar{1}$-$I2/c$ phase transition in alkaline-earth feldspars along the $CaAl_2Si_2O_8$-$SrAl_2Si_2O_8$ join: Thermodynamic behavior. Physics and Chemistry of Minerals, 20, 221–227.

Vallade, M., Berge, B., and Dolino, G. (1992) Origin of the incommensurate phase of quartz: II. Interpretation of inelastic neutron scattering data. Journal de Physique, I-2, 1481–1495.

Warren, J.L., and Worton, T.G. (1974) Improved version of group-theoretical analysis of lattice dynamics. Computer Physics Communications, 8, 71–84.

Welberry, T.R., Hua, G.L., and Withers, R.L. (1989). An optical transform and Monte Carlo study of the disorder in β-cristobalite SiO_2. Journal of Applied Crystallography, 22, 87–95.

Wennemer, M., and Thompson, A.B. (1984) Tridymite polymorphs and polytypes. Schweizerische Mineralogische und Petrographische Mittilungen, 64, 335–353.

Winkler, B., Dove, M.T., and Leslie, M. (1991) Static lattice energy minimization and lattice dynamics calculations on aluminosilicate minerals. American Mineralogist, 76, 313–331.

Withers, R.L., Thompson, J.G., and Welberry, T.R. (1989) The structure and microstructure of α-cristobalite and its relationship to β-cristobalite. Physics and Chemistry of Minerals, 16, 517–523.

Withers, R.L., Thompson, J.G., Xiao, Y., and Kirkpatrick, R.J. (1994) An electron diffraction study of the polymorphs of SiO_2-tridymite. Physics and Chemistry of Minerals, 21, 421–433.

Wright, A.F., and Leadbetter, A.J. (1975) The structures of the β-cristobalite phases of SiO_2 and $AlPO_4$. Philosophical Magazine, 31, 1391–1401.

Manuscript received July 11, 1995
Manuscript accepted June 3, 1996